

# A BUDGET AND ACCOUNTING OF METALS AT $Z \sim 0$ : RESULTS FROM THE COS-HALOS SURVEY<sup>1</sup>

MOLLY S. PEEPLES<sup>2,3</sup>, JESSICA K. WERK<sup>4</sup>, JASON TUMLINSON<sup>3</sup>,  
BENJAMIN D. OPPENHEIMER<sup>5,6</sup>, J. XAVIER PROCHASKA<sup>4</sup>, NEAL KATZ<sup>7</sup>, DAVID H. WEINBERG<sup>8</sup>

*Draft version October 31, 2018*

## ABSTRACT

We present a budget and accounting of metals in and around star-forming galaxies at  $z \sim 0$ . We combine empirically derived star formation histories with updated supernova and AGB yields and rates to estimate the total mass of metals produced by galaxies with present-day stellar mass of  $10^{9.3} - 10^{11.6} M_{\odot}$ . On the accounting side of the ledger, we show that a surprisingly constant 20–25% mass fraction of produced metals remain in galaxies’ stars, interstellar gas and interstellar dust, with little dependence of this fraction on the galaxy stellar mass (omitting those metals immediately locked up in remnants). Thus, the bulk of metals are outside of galaxies, produced in the progenitors of today’s  $L^*$  galaxies. The COS-Halos survey is uniquely able to measure the mass of metals in the circumgalactic medium (to impact parameters of  $< 150$  kpc) of low-redshift  $\sim L^*$  galaxies. Using these data, we map the distribution of CGM metals as traced by both the highly ionized O VI ion and a suite of low-ionization species; combined with constraints on circumgalactic dust and hotter X-ray emitting gas out to similar impact parameters, we show that  $\sim 40\%$  of metals produced by  $M_{\star} \sim 10^{10} M_{\odot}$  galaxies can be easily accounted for out to 150 kpc. With the current data, we cannot rule out a constant mass of metals within this fixed physical radius. This census provides a crucial boundary condition for the eventual fate of metals in galaxy evolution models.

*Keywords:* galaxies: abundances, halos — intergalactic medium — quasars: absorption lines

## 1. INTRODUCTION

As all elements heavier than boron are produced by stars and supernovae, the eventual fate of heavy elements (“metals”) is a unique boundary condition for galaxy evolution models. Stellar winds and supernovae expel metals into the interstellar medium (ISM) or from galaxies via large-scale outflows. The metal-enriched ISM continues to cool, collapse, and form new stars, thereby trapping some metals in stars. The relative distribution of metals in stars, in the ISM, and outside of galaxies is highly sensitive to galaxies’ star formation histories, outflow histories, and the depths of their potential wells. We present here an empirical budget and accounting of metals both inside of star-forming galaxies and in the surrounding circumgalactic medium (CGM) at  $z \sim 0$  as a function of galaxy mass.

Early attempts to take census of metals at higher redshifts (Pettini 1999; Ferrara et al. 2005; Bouché et al. 2005, 2006, 2007) found that the bulk of metals pro-

duced by these galaxies have been expelled by  $z \sim 2$ . Contemporary studies of  $0.5 \lesssim z \lesssim 5$  damped Lyman- $\alpha$  systems, despite their being a biased tracer of cosmic metals, likewise inferred metal mass densities a factor of ten lower than that expected from the star formation history of the universe (Prochaska et al. 2003). Given the near-ubiquity of galaxy-scale outflows at these redshifts (Shapley et al. 2003; Weiner et al. 2009), it follows that the majority of metals produced in galaxies may have been transported away from their stellar components (see also Lehner et al. 2014). At lower redshifts, Gallazzi et al. (2008) found that disk-dominated, i.e., presumably star-forming, galaxies have less than 25% of their metals in stars. Bouché et al. (2007) suggested that at  $z \sim 0$  there could be as many metals in an O VI-traced warm-hot intergalactic medium (WHIM) as in stars (cf. Pagel 2008). Following these ideas, Zahid et al. (2012b) combined an estimate of oxygen masses in stars and the interstellar medium at  $z \sim 0$ , finding that the mass of oxygen expelled from  $\log M_{\star}/M_{\odot} \sim 11$  galaxies is higher than the lower limit given by the O VI-traced CGM oxygen mass found by Tumlinson et al. (2011). From a theoretical standpoint, highly efficient winds that remove large amounts of freshly produced metals are necessary to understand the ISM abundances of both local and high-redshift galaxies (e.g., Dalcanton 2007; Erb 2008; Finlator & Davé 2008; Arrigoni 2010; Peeples & Shankar 2011; Davé et al. 2011; Dayal et al. 2013). Similarly, outflows appear necessary to reach the level of observed CGM and intergalactic medium (IGM) metal enrichment (Oppenheimer & Davé 2006; Scannapieco et al. 2006; Shen et al. 2010, 2012; Booth et al. 2012; Oppenheimer et al. 2012; Stinson et al. 2012; Ford et al. 2013; Crain et al. 2013; Berry et al. 2013).

Though it is possible that a significant fraction of cos-

molly@stsci.edu

<sup>1</sup>Based on observations made with the NASA/ESA Hubble Space Telescope, obtained at the Space Telescope Science Institute, which is operated by the Association of Universities for Research in Astronomy, Inc., under NASA contract NAS 5-26555. These observations are associated with program GO11598.

<sup>2</sup>Southern California Center for Galaxy Evolution Fellow, Department of Physics and Astronomy, University of California, Los Angeles, Los Angeles, CA

<sup>3</sup>Space Telescope Science Institute, Baltimore, MD

<sup>4</sup>UCO/Lick Observatory, University of California, Santa Cruz, CA

<sup>5</sup>CASA, Department of Astrophysical and Planetary Sciences, University of Colorado, Boulder, CO

<sup>6</sup>Leiden Observatory, Leiden University, the Netherlands

<sup>7</sup>Department of Astronomy, University of Massachusetts, Amherst, MA

<sup>8</sup>Department of Astronomy, The Ohio State University, Columbus, OH

mic metals are in the CGM and IGM, it has been difficult to do a full accounting in the low redshift Universe. Rest-frame UV spectra—and thus space-based observations—are needed in order to probe the dominant ionic transitions and infer column densities, mass budgets, and kinematics. The COS-Halos survey (GO 11598; PI J. Tumlinson) was defined to address this problem with a sample of 44 galaxies observed by HST/COS along QSO sightlines passing within 150 physical kpc of  $z \sim 0.25$  galaxies over a range of stellar mass and star formation properties. The rationale and design for COS-Halos are described in Tumlinson et al. (2013); the key findings on metal lines are found in Tumlinson et al. (2011) for high-ionization gas and in Werk et al. (2013) for low-ionization gas. Tumlinson et al. (2011) reported that the mass of oxygen traced by the highly ionized O VI in the CGM of star-forming galaxies is comparable to the mass of oxygen in their ISM. COS-Halos has specifically addressed the metal content of diffuse halo gas. The current study aims to place these findings on highly ionized oxygen into the larger context of metal masses contained within all galactic and circumgalactic components: stars, dust, and the other gaseous components; we also for the first time assess the metal mass in the lower-ionization state CGM using the COS-Halos data.

By  $z = 0$  the bulk of heavy elements that have ever been produced are locked up in stellar remnants, such as white dwarfs or neutron stars. This inventory, however, is dominated by metals that have never been processed through the interstellar medium, and are instead directly locked up in these remnants shortly after being produced (Fukugita et al. 1998; Fukugita & Peebles 2004). As we are interested here in constraining large-scale gas flows and galaxy evolution processes, we ignore those metals that are produced in stars but immediately locked into compact remnants, and consider only those heavy elements that have been expelled into the ISM by supernovae and stellar winds.

Traditionally, the so-called “missing metals problem” has been phrased by comparing the summed-up cosmic density of metals that produced by the previous epochs of star formation to the cosmic density of metals accounted for in stars the ISM, and the IGM; these comparisons show that somewhere between 35 and 90% of metals are unaccounted for (e.g., Ferrara et al. 2005; Bouché et al. 2007; Pagel 2008). This large range stems from uncertainties in the cumulative star formation rate and the cosmic density of metals in different components. Here, we instead consider the distribution of metals produced in star-forming galaxies as a function of stellar mass; this approach allows us to systematically consider how uncertainties in input scaling relations affect our census in different galaxy mass ranges. Moreover, a mass-dependent metal inventory lends insight into how galaxies with differing histories of star formation and outflow efficiency have redistributed their metals differently through cosmic time.

We begin our census in § 2 with the budget of available metals from supernovae and asymptotic giant branch (AGB) stars. In § 3 we consider the metals that are still in galaxies, and in § 4 we turn to those metals observed in the circumgalactic medium. We consider possible uncertainties in these measurements as we assess the severity of the missing-metals problem in § 5, and we summarize

our conclusions in § 6. In the Appendix, we address the implications of a non-global  $[\alpha/\text{Fe}]$  ratio with a similar accounting for oxygen.

Throughout we assume a Chabrier (2003a) initial mass function (IMF). Our choice of IMF mainly affects our inferred rates of metal production via, for example, the supernova rate relative to the star formation rate. We also assume that all galaxies have—and have always had—this same IMF, though there is increasing evidence in the literature that the true picture may be more complicated (e.g., Auger et al. 2010; Brewer et al. 2012; Conroy & van Dokkum 2012; Sonnenfeld et al. 2012; Dutton et al. 2013; Geha et al. 2013). Where relevant, we adopt Solar abundances from Caffau et al. (2011) and Lodders et al. (2009).

## 2. THE BUDGET OF AVAILABLE METALS

We first turn to the  $z \sim 0$  metal budget, i.e., how many metals have galaxies made available? We consider the entire inventory of metals ejected from stars through processes including explosive supernovae and stellar winds. We ignore metals that remain locked in stellar remnants including white dwarfs, neutron stars, and black holes. Though these sources comprise the majority of metals ever produced over cosmic time (Fukugita & Peebles 2004), doing a precise and accurate budget and accounting for remnants is difficult, and is insensitive to the questions of galaxy gas flows that we wish to address here.<sup>9</sup>

By mass, roughly 80–85% of the metals made come from core-collapse supernovae (§ 2.1), with the rest being made by Type Ia supernovae (§ 2.2) and AGB stars (§ 2.3). In contrast, essentially all of the oxygen comes from core-collapse supernovae, with the small contribution made by Type Ia supernovae subsequently destroyed by AGB stars in massive galaxies. The black line in Figure 1 shows all of the metals produced, i.e.,  $M_{z,\text{ii}} + M_{z,\text{ia}} + M_{z,\text{agb}}$ , with the shaded grey region denoting our adopted uncertainties, as described below. (The colored regions denote metals in galaxies, as described in § 3.)

The mass of metals produced by a galaxy depends on its historical rates of Type II supernovae, Type Ia supernovae, and AGB stars. While these rates can be estimated from the  $z = 0$  stellar mass, each is explicitly tied to the galaxy’s star formation history. Therefore, we use star formation histories derived by Leitner (2012) to model the rates of metal production.<sup>10</sup> By assuming that star-forming galaxies have evolved along the mean observed star forming sequence (i.e., the evolving  $\dot{M}_{\text{sfr}}-M_{\star}$  relation), Leitner derived star formation rates as a function of redshift for  $z = 0$  galaxies. This straightforward empirical model works well to reproduce the star formation histories inferred from the fossil record of  $\sim L^*$  galaxies, although it does predict too *much* downsizing for  $M_{\star,0} \lesssim 10^9 M_{\odot}$  galaxies (i.e., it predicts that these dwarf galaxies have formed all of their stars at late times, contrary to what is observed). Fortunately, the bulk of

<sup>9</sup> Throughout this paper, when we refer to the mass of metals “made”, “produced”, or “available”, we are implicitly ignoring the metals directly locked up in remnants and instead only considering those metals expelled by supernovae and AGB stars.

<sup>10</sup> We note that Leitner (2012) adopts a slightly different cosmology than used for the COS-Halos sample in § 4, but that this should not have a substantial effect on our results.

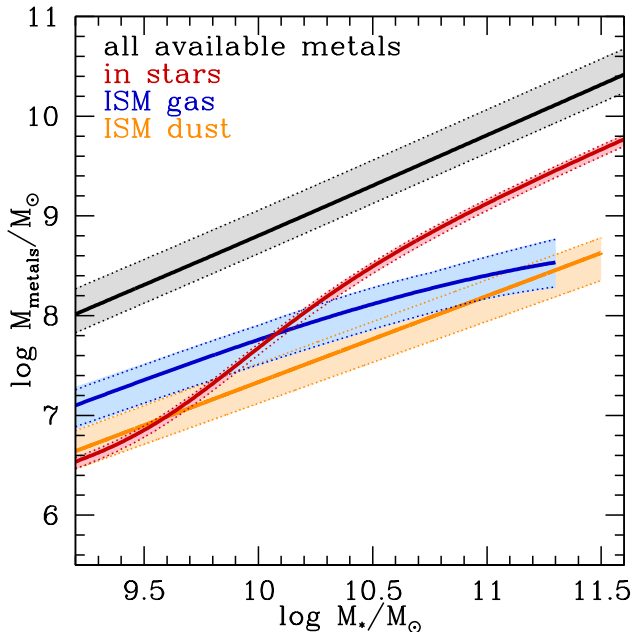


**Figure 1.** The total mass of metals produced by supernovae and AGB stars (§ 2; black), the mass of metals currently in stars (§ 3.1; red), the mass of metals in interstellar gas (§ 3.2; blue), and the mass of metals in dust (§ 3.3; orange), all plotted vs. the  $z = 0$  galactic stellar mass of star-forming galaxies. The shaded regions and dotted lines denote the adopted uncertainties as discussed in the text.

metals are produced through core-collapse supernovae, and the final mass of metals produced by Type II supernovae depend more sensitively on the total mass of stars formed than on the precise history of when the stars formed (unlike the products of Type Ia supernovae or AGB stars). Hence, our results are not very dependent on the assumed star formation histories, although these histories do provide a useful framework for examining the sources of metals in galaxies of different mass.

### 2.1. Core-collapse Supernovae

The mass of metals made by Type II supernovae (i.e., core-collapse supernovae) is

$$M_{Z,ii} = \int y_{z,ii} \dot{M}_{\text{sfr}} dt \quad (1)$$

where  $\dot{M}_{\text{sfr}}$  is the rate at which stars of mass  $0.1$ – $100 M_{\odot}$  are being made, and  $y_{z,ii}$  is the nucleosynthetic yield of all heavy elements produced by Type II supernovae. Because not all stars made survive to  $z = 0$  (i.e.,  $M_{\star,0} < \int \dot{M}_{\text{sfr}} dt$ ), the mass of metals made by Type II supernovae is higher than  $y_{z,ii} M_{\star,0}$ , where  $M_{\star,0}$  is the galaxy mass at  $z = 0$ . Specifically, using the star formation histories provided by Leitner (2012), we find that the Type II supernova metal production can be well described as

$$\log(M_{Z,ii}/M_{\odot}) = 1.0146 \log(M_{\star,0}/M_{\odot}) + \log y_{z,ii} + 0.1091. \quad (2)$$

Note that this relation is not very dependent on the assumed star formation history; that is, the slope is nearly unity. For the mass range we consider here, this is quite close to just assuming that all galaxies have recycled  $\sim$

55% of their stellar mass (i.e.,  $\int \dot{M}_{\text{sfr}} dt \sim 1.8 \times M_{\star,0}$ ),<sup>11</sup> which for a Chabrier (2003a) IMF is very similar to the commonly used “instantaneous recycling approximation” for all stars  $m > 1 M_{\odot}$ .

We adopt nucleosynthetic yields of  $y_{z,ii} = 0.030$ , with the main elemental contributions having yields of 0.015 (oxygen), 0.0083 (carbon), 0.0014 (silicon), 0.0011 (iron), and 0.001 (nitrogen). These values are in the middle of the range we derive from the non-primordial models of Woosley & Weaver (1995), Portinari et al. (1998), Chieffi & Limongi (2004), and Hirschi et al. (2005), under the assumption that stars of mass  $10 < m < 100 M_{\odot}$  end as core-collapse supernovae. Our adopted yields are close to those given by Chieffi & Limongi (2004). The grey shaded region in Figure 1 includes the effects of letting our assumed yields vary within the ranges given by the models: we let  $y_{z,ii}$  vary from 0.0214 to 0.0408, and let  $y_{o,ii}$  vary from 0.01394 to 0.01828 (see the Appendix). Woosley & Weaver tend to give lower  $y_{z,ii}$  than the more recent models; we note that this means our fiducial yields are somewhat higher than those assumed in earlier chemical evolution models (e.g., Madau et al. 1996; Ferrara et al. 2005). On the other hand, the only model that includes stellar rotation (Hirschi et al. 2005) gives a much higher metal yield than those neglecting rotation. As the models give little dependence of the yield on the progenitor metallicity—especially given the full range of uncertainty in the above models—we do not take into account a galaxy’s metallicity history and instead assume that the yields do not vary.

For a single population of stars with mass  $0.1 < m < 100 M_{\odot}$  formed with a Chabrier (2003a) IMF, 18.58% of the mass is in stars with  $10 < m < 100 M_{\odot}$  and 21.16% in stars with  $8 < m < 100 M_{\odot}$ .<sup>12</sup> The uncertainties shown in Figure 1 include the effects of letting the minimum supernova mass vary from  $8 M_{\odot}$  to  $10 M_{\odot}$ .

### 2.2. Type Ia Supernovae

We adopt a  $t^{-1}$  delay time distribution for Type Ia supernovae, where

$$\text{SNR}(t)_{\text{Ia}} = 4 \times 10^{-13} \text{ yr}^{-1} m_{\star} \left( \frac{t}{1 \text{ Gyr}} \right)^{-1} \quad (3)$$

is the rate of Type Ia supernovae produced by a stellar population of mass  $m_{\star}$  formed at time  $t = 0$  (Maoz & Mannucci 2012). The metal production from Type Ia supernovae is then described by

$$M_{Z,\text{ia}} = \int m_{z,\text{ia}} \text{SNR}_{\text{Ia}} dt, \quad (4)$$

where  $m_{z,\text{ia}} = 1.2256 M_{\odot}$  is the mass of metals produced per Type Ia supernova; in the Appendix, we assume that each Type Ia supernova produces  $0.143 M_{\odot}$  of oxygen (Thielemann et al. 1986; Tsujimoto et al. 1995). Fifty percent of the total metal mass is in the form of iron. The mass of metals oxygen produced by Type Ia supernovae are well described as

$$\log(M_{Z,\text{ia}}/M_{\odot}) = 1.043 \log(M_{\star,0}/M_{\odot}) - 2.683. \quad (5)$$

<sup>11</sup> More specifically,  $1.0146 \times 10 + \log y_{z,ii} + 0.1091 \approx 10 + \log 1.8 + \log y_{z,ii}$ .

<sup>12</sup> These fractions will be lower by a factor of  $\sim 3$  for a Salpeter (1955) IMF.

Though the Type Ia metal production is more dependent on the assumed star formation histories than it is for core-collapse supernovae (§ 2.1), because Type Ia supernovae are responsible for only  $\sim 10\%$  of the metals, uncertainties in the star formation histories or Type Ia supernova rates do not strongly affect our integrated results. The grey shaded region in Figure 1 takes into account a factor of two uncertainty in the Type Ia supernova rate (Maoz & Mannucci 2012) and lets the masses of metals produced vary by a factor of two (Gibson et al. 1997).

### 2.3. Asymptotic Giant Branch Stars

Metal processing by AGB stars depends sensitively on their mass and initial metallicity (e.g., Karakas 2010). Following Peeples & Somerville (2013), we determine a galaxy’s evolving metallicity by assuming that as galaxies form stars according to the Leitner (2012) star formation histories, the ISM metallicity remains on the observed  $z \sim 0$  relation between stellar mass, star formation rate, and gas-phase metallicity as measured by Mannucci et al. (2010). This assumption is motivated by the fact that observed galaxies at  $0 \lesssim z \lesssim 2.2$  all appear to lie on the same relation. Peeples & Somerville (2013) showed that this simple approach for modeling galaxy metallicity histories reproduces the  $z = 0$  stellar metallicities as measured by Gallazzi et al. (2005) and Woo et al. (2008) rather well.

We adopt the AGB metal yield look-up tables as tabulated by Oppenheimer & Davé (2008) for their Gadget-2 simulations and apply those yields to our model star formation histories, assuming a factor of two uncertainty in the yields. They tabulated AGB yields from stellar models of different input masses and metallicities calculated by Marigo (2001), Herwig (2004), and Gavilán et al. (2005), and converted from stellar mass to age using stellar lifetimes, since the AGB phase occurs right before stellar death. We use these tables as a function of age and metallicity to calculate the amount of carbon, nitrogen, and oxygen produced by stars dying at each  $1.3 \times 10^7$  yr time step using the Leitner (2012) star formation histories and the Peeples & Somerville (2013) stellar metallicities. We are interested in the total amount of C, N, and O “processed” by the AGB stars, which is the ejected metal mass in excess of the metals present in the star at birth. Significant amounts of carbon and nitrogen are produced in AGB stars compared to Type II SNe production. Oxygen can be lost via AGB stars because this element is burned, remaining trapped in the remnant, in many AGB stars (Karakas et al. 2012). However, the net loss is small compared to the amount of oxygen produced by Type II SNe. Over the mass range and for the AGB models we consider here, oxygen is primarily destroyed in AGB stars, and the total change in metal mass owing to AGB processing is mainly from added carbon mass. Other metals are not significantly processed by AGB stars when considering the mass of all metals: metals heavier than oxygen mostly remain unprocessed, while the species with the largest changes are rare isotopes by mass (e.g.  $^{13}\text{C}$ ).

### 2.4. Summary: Metal Budgets

Figure 2 shows the breakdown of metal production sources by element (O, C, Fe, Si, and N) as a function

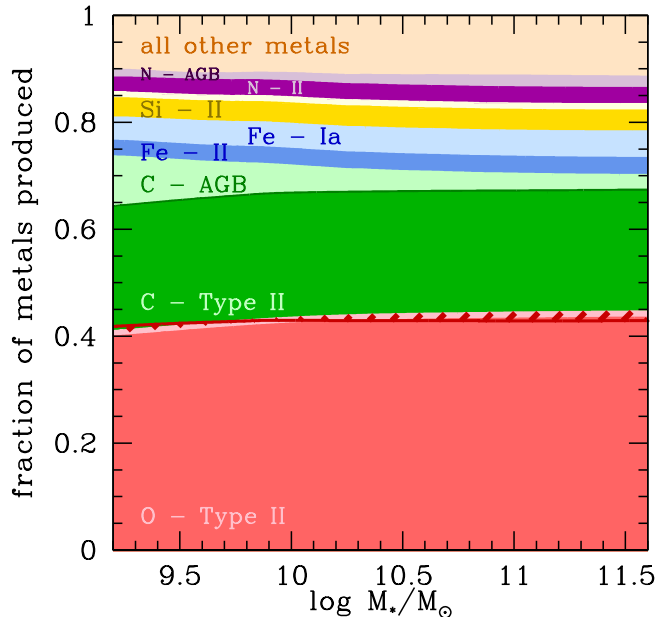


**Figure 2.** The cumulative fraction of metals produced by  $z = 0$ , broken down by element and source vs. the galaxy stellar mass. As most metals are produced in Type II supernovae, the variations in elemental fraction with respect to stellar mass due to varying star formation histories in contributions from Type Ia SNe and AGB stars are relatively small. The most abundant element is oxygen (dark pink, Type II SNe; light pink, Type Ia SNe; dark red hashed, AGB, showing the destruction of oxygen in more massive galaxies), followed by carbon (medium green, Type II SNe; dark green, Type Ia SNe; pale green, AGB), iron (dark blue, Type II SNe; pale blue, Type Ia SNe), silicon (dark yellow, Type II SNe; pale yellow, Type Ia SNe), and nitrogen (dark purple, Type II SNe; pale purple, AGB). The contribution from other elements is  $\sim 10\%$  (pale orange).

of  $M_{*,0}$ . Interestingly, the expected fraction in oxygen is very close to the Solar value of  $\sim 44\%$ ; in fact, to within a few percent, the pattern shown in Figure 2 is close to the Solar abundance pattern, with the obvious exception of Carbon (the Solar C/Z is  $\approx 18\%$  as opposed to the  $\sim 30\%$  shown in Fig. 2). We note, however, that in addition to the AGB yields being highly uncertain, the channel for carbon production from core-collapse supernovae is poorly understood; among the different supernova models we considered, the carbon yield varies by over a factor of 4 (as opposed to the factor of  $< 2$  for all metals).

### 3. HOW MANY METALS ARE STILL IN GALAXIES?

We now turn to an accounting of metals at  $z \sim 0$  by considering those metals that are in galaxies. The metals in galaxies are shown in Figure 1: we consider metals in stars (red, § 3.1), the neutral interstellar medium (ISM; blue, § 3.2), or interstellar dust (orange, § 3.3). As elsewhere in this paper, we assume here that we can use mean scaling relations to describe a “typical” galaxy and that the scatter about these scaling relations does not affect our conclusions about these typical galaxies. For the largest two contributors, stars and the ISM, the relevant observations are from the Sloan Digital Sky Survey (SDSS); thus we further assume that the  $3''$  subtended by SDSS fibers are representative of the global stellar or gaseous metallicities (and that accurate aperture corrections have been made).

### 3.1. Stars

The mass of metals in stars at  $z = 0$  of a galaxy with stellar mass  $M_{\star,0}$  is

$$M_{Z,\star} = Z_{\star} M_{\star,0}. \quad (6)$$

The observed stellar metallicity  $Z_{\star}$  is weighted by the most luminous stars in the galaxy, which are also the youngest, and, therefore, most metal rich stars. [Peeples & Somerville \(2013\)](#) traced the buildup of metals in stars by following the [Leitner \(2012\)](#) star formation histories (see §2.3). Using the stellar population synthesis models of [Bruzual & Charlot \(2003\)](#) they compared the  $B$ -band weighted stellar metallicities,  $Z_{\star,\text{light}}$ , to the more physical mass-weighted stellar metallicities,  $Z_{\star,\text{mass}}$ . This correction is well fit by the power law

$$\log(Z_{\star,\text{mass}}/Z_{\odot}) = 1.08 \log(Z_{\star,\text{light}}/Z_{\odot}) - 0.16. \quad (7)$$

We correct the observed stellar metallicities to a mass-weighted value using equation (7).

The red line in Figure 1 denotes the mass of metals locked up in stars, as a function of  $M_{\star}$ , using the  $Z_{\star}$  measurements from [Gallazzi et al. \(2005\)](#); uncertainties in these descriptions of “typical”  $Z_{\star}$  are not shown. We use equation (7) to convert from luminosity-weighted observations to the actual masses. The band shows the uncertainty in the solar abundance. We adopt  $Z_{\odot} \equiv M_{Z,\odot}/M_{\odot} = 0.0153$  from [Caffau et al. \(2011\)](#) and show the range of  $Z_{\odot} = 0.013$  to  $0.0168$  from [Bahcall et al. \(2005\)](#) as possible sources of uncertainty. Compared to the uncertainties relevant to other components, the contribution from the uncertainty in the Solar abundance is small. [Gallazzi et al. \(2005\)](#) give an uncertainty of  $\sim 0.12$  dex in metallicity for each galaxy, though their stated medians have much smaller uncertainties.

### 3.2. Interstellar Gas

The mass of metals in the interstellar medium at  $z = 0$  is simply

$$M_{Z,\text{ISM}} = Z_{\text{g}} M_{\text{g}}, \quad (8)$$

where  $Z_{\text{g}}$  is the metallicity of the ISM and  $M_{\text{g}}$  is the galaxy gas mass. Generally the radial metallicity gradients in spiral galaxies at large radius are shallow, implying that the gas is well-mixed ([Cartledge et al. 2004](#); [Werk et al. 2011](#)). Hence, for the gas masses, we include all of the cold gas, i.e., everything that is traced by H I plus molecular gas.

In Figure 3 we show the atomic plus molecular gas mass measurements from [McGaugh \(2005, 2012\)](#) and [Leroy et al. \(2008\)](#), adding star-forming ( $\text{NUV} - r < 4$ ) galaxies from the COLDGASS sample ([Saintonge et al. 2011](#)). We list the median, 16- and 84% ranges of these data in bins of stellar mass in Table 1. A least-squares fit to the full data set gives us the gas fractions as a function of stellar mass,

$$\log F_{\text{g}} \equiv \log(M_{\text{g}}/M_{\star}) = -0.48 \log M_{\star} + 4.39. \quad (9)$$

Using a similar approach, [Papastergis et al. \(2012\)](#) find

$$\log F_{\text{g}} = \log(1.366 M_{\text{HI}}/M_{\star}) = -0.43 \log M_{\star} + 3.89, \quad (10)$$

by fitting a power law to data compiled from optically-selected galaxy samples ([Swaters & Balcells 2002](#);

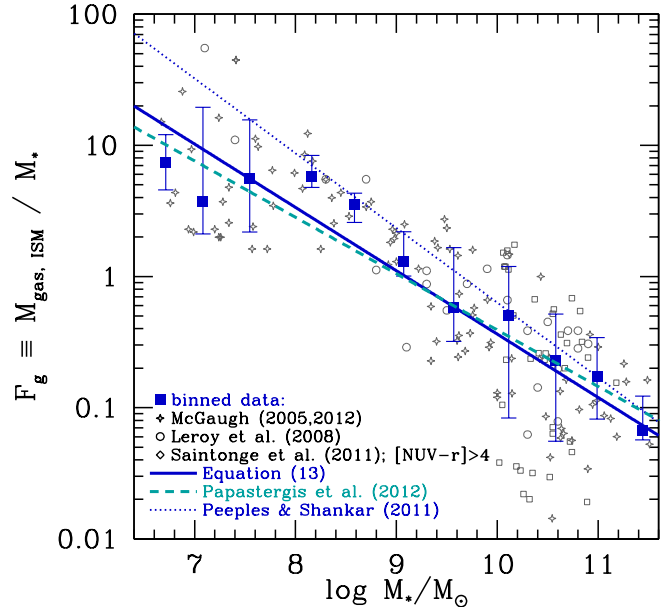


**Figure 3.** Cold (atomic + molecular) gas fractions,  $F_{\text{g}} \equiv M_{\text{g}}/M_{\star}$ , as a function of stellar mass. The grey data points are collated from [McGaugh \(2005, 2012\)](#), [Leroy et al. \(2008\)](#), and [Saintonge et al. \(2011\)](#), with selections for star-forming galaxies and a conversion to a [Chabrier \(2003b\)](#) IMF where appropriate. The blue points are the median  $F_{\text{g}}$  in bins of  $\Delta \log M_{\star} = 0.5$  dex, with errorbars denoting the 16- to 84% range of the data, as tabulated in Table 1. The solid blue line is a fit to the data (equation 9); the dashed cyan line is an independent fit to similar data from [Papastergis et al. \(2012\)](#), see also equation 10). For comparison we also show the “total” gas fractions from [Peeples & Shankar \(2011\)](#) (dotted blue line), which strongly over-estimates the gas fractions for dwarf galaxies.

[Garnett 2002](#); [Noordermeer et al. 2005](#); [Zhang et al. 2009](#)). We convert their  $M_{\text{HI}}$  to the total gas mass by setting  $M_{\text{g}} = 1.366 M_{\text{HI}}$  to correct for He, by adopting the Solar value for the mean atomic weight of 1.366 ([Caffau et al. 2011](#)). We use the average of the gas masses given by these two fits and the uncertainty ranges in Figure 1 take into account the (small) range these fits span at higher  $M_{\star,0}$ .

We note that [Peeples & Shankar \(2011\)](#) gave gas fractions that were biased high (dotted blue line in Figure 3) because many galaxies in their sample were H I-selected ([West et al. 2009, 2010](#)), which led to an overestimate of  $F_{\text{g}}$  at fixed  $M_{\star}$  ([Papastergis et al. 2012](#)). Moreover, their “total” fit was also offset by  $+0.2$  dex (for illustrative purposes) and was steeper than what we find here. The fits given by equations (9) and (10) are also lower than those derived from the [Peeples & Shankar \(2011\)](#) binned data, as done by, e.g. [Zahid et al. \(2012b\)](#). We provide an update to these binned data in Table 1. As the mass of metals in the ISM is proportional to the gas mass (equation 8), these seemingly small differences can have a large impact on the missing-metals problem, especially for gas-rich dwarf galaxies.

In addition to the cold atomic and molecular gas traced by the data shown in Figure 3, the Milky Way has a warm ionized medium (WIM) that may harbor a similar total and metallic mass as that in neutral gas ([Sembach et al. 2000](#); [Haffner et al. 2009](#)). However, systematic characterizations of the mass in this phase for galaxies other than our own are rare, and it is unclear how well the WIM mass scales with either H I or stellar mass ([Oey et al.](#)

$\langle \log M_\star \rangle$	median $F_g$	16%ile $F_g$	84%ile $F_g$
6.7	7.4	12.0	4.6
7.1	3.7	19.5	2.1
7.6	5.6	15.7	2.2
8.2	5.8	8.4	4.8
8.6	3.6	4.3	2.6
9.1	1.3	2.2	1.0
9.6	0.6	1.7	0.32
10.1	0.50	1.2	0.083
10.6	0.23	0.52	0.056
11.0	0.17	0.34	0.082
11.4	0.067	0.12	0.057

**Table 1**

Median, 16-, and 84-percentile cold gas fractions  $F_g \equiv M_g/M_\star$  in bins of  $\Delta \log M_\star = 0.5$  dex for the [McGaugh \(2005, 2012\)](#), [Leroy et al. \(2008\)](#), and [Saintonge et al. \(2011\)](#) data sets, as shown in [Figure 3](#).

2007). Furthermore, the relative amounts of ionized versus neutral gas will naturally depend on the ambient ionization fields. We, therefore, stress that the metal masses we quote here for “the interstellar medium” apply *only* to the cold gas, and that the total interstellar gaseous metal masses could be larger by as much as a factor of two.

On the other hand, because the typical  $z \sim 0$  galaxy could have a shallow metallicity gradient, or gas that is not entirely well-mixed, the  $M_g$  and thus the  $M_{Z,\text{ISM}}$  that we adopt here should be considered as upper-limits to the amount of metals in the cold interstellar medium, especially at the lowest  $M_\star$ , where galaxies often have very extended H I envelopes relative to their stars.

### 3.2.1. Oxygen in the ISM

The largest and most standardized surveys of ISM metallicities relative to galaxy stellar mass are that of oxygen abundances measured from nebular emission lines in H II regions. Systematic uncertainties in theoretical photoionization models and empirical calibrations, however, lead to dramatically different measurements for  $\log(\text{O}/\text{H})$  for the same set of emission line fluxes; we refer the reader to the review by [Kewley & Ellison \(2008\)](#) for a detailed discussion of these issues.<sup>13</sup> Using SDSS spectra, [Kewley & Ellison \(2008\)](#) give fits to ten mass-metallicity relations derived from different abundance calibrations in the literature. We take the average of the eight most similar relations (dropping the two with the lowest calibrations and flattest slopes, both of which are based on  $T_e$  measurements tied to the [O III]  $\lambda 4363$  line that are known to give systematically low estimates of O/H). These calibrations typically assume a 0.1 dex depletion of oxygen onto dust; as we wish to isolate the *gas*-phase oxygen abundance, we subtract 0.1 dex from each of these calibrations, adopting

$$\log \frac{M_{\text{oxy,ism}}}{M_g} = 27.76 - 7.056 \log M_\star \quad (11)$$

$$+ 0.8184(\log M_\star)^2 - 0.03029(\log M_\star)^3, \quad (12)$$

<sup>13</sup> These systematic uncertainties are expected to be resolved by adopting a  $\kappa$ -distribution rather than a Maxwell-Boltzmann distribution for electron energies ([Nicholls et al. 2012](#); [Dopita et al. 2013](#)).

where  $M_\star$  is in units of  $M_\odot$ , and

$$\frac{M_{\text{oxy,ism}}}{M_g} = \frac{m_{\text{O}} \times n_{\text{oxy}}}{\bar{\mu} m_p \times n_{\text{H}}} = \frac{15.999}{1.366} \times \frac{n_{\text{oxy}}}{n_{\text{H}}}, \quad (13)$$

where  $n_{\text{oxy}}/n_{\text{H}}$  is the number abundance of oxygen relative to hydrogen as expressed by  $12 + \log(\text{O}/\text{H})$ ,  $m_p$  is the mass of a proton,  $m_{\text{O}} = 15.999m_p$  is the mass of an oxygen atom, and we adopt the Solar value of  $\bar{\mu} = 1.366$  ([Caffau et al. 2011](#)).

### 3.2.2. Metals in the ISM

Stars show a variation in  $[\alpha/\text{Fe}]$  relative to galactic stellar mass (see [§ A.1](#)). Similarly, star formation driven outflows are reasonably expected to be  $\alpha$ -enhanced (as they are presumably primarily driven by Type II supernovae, the primary sites of  $\alpha$ -element formation), and the efficiency of such outflows in removing metals from the ISM should vary as a function of galaxy mass (e.g., [Murray et al. 2005](#); [Peeples & Shankar 2011](#)). It is, therefore, quite possible that the interstellar  $[\alpha/\text{Fe}]$  varies as a function of stellar mass. However, as definitive observations one way or the other do not exist, we therefore adopt a Solar oxygen-to-metals ratio of  $0.00674/0.0153 = 0.44$  for the ISM. The width of the blue band in [Figure 1](#) denotes the uncertainty in  $M_{Z,\text{ISM}}$  and almost entirely owes to uncertainties in the  $12 + \log(\text{O}/\text{H})$  calibration ([§ 3.2.1](#)).

### 3.3. Interstellar Dust

Though the absolute mass of dust in galaxies is small compared to the total mass of stars and the ISM, dust is (by mass) almost entirely composed of heavy elements. [Figure 4](#) shows measured dust masses as a function of stellar mass from the Spitzer Infrared Nearby Galaxies Survey (SINGS; [Draine et al. 2007](#)), with stellar masses from [da Cunha et al. \(2008\)](#)<sup>14</sup> and from the Herschel KINGFISH survey ([Skibba et al. 2011](#)).<sup>15</sup> These samples were selected to be representative of normal galaxies at  $z \sim 0$  ([Kennicutt et al. 2003](#)); therefore, their dust masses should not be abnormally high (or low). These two samples have 40 star-forming (which we define as  $\dot{M}_{\text{sfr}}/M_\star > 10^{-11} \text{ yr}^{-1}$ ) galaxies in common. The average of the two sets of measured stellar and dust masses are shown in orange. We adopt the fit to the averaged data, also shown in orange,

$$\log(M_{\text{dust}}/M_\odot) = 0.86 \log(M_{\star,0}/M_\odot) - 1.31. \quad (14)$$

Relative to the gas fractions given in [Equation \(9\)](#), this results in a dust-to-gas ratio<sup>16</sup> of  $\sim 1\%$  at  $M_{\star,0} \sim 10^{10.5} M_\odot$  and a dust-to-metals ratio of  $\sim 30\text{--}50\%$ . The uncertainty range shown in [Figure 1](#) corresponds to the two independent fits; the dotted lines are the fits to the full data samples, and the solid lines are the independent fits to the overlapping galaxies. We note that only 15 of the overlapping galaxies have SCUBA sub-mm data and

<sup>14</sup> We thank E. da Cunha for sharing these stellar mass measurements with us.

<sup>15</sup> We have corrected the [Skibba et al. \(2011\)](#) stellar masses by  $-0.05$  dex to convert them from a [Kroupa \(2001\)](#) IMF to [Chabrier \(2003b\)](#) IMF ([Bernardi et al. 2010](#)).

<sup>16</sup> The dust masses are measured independently of the galaxy gas masses.

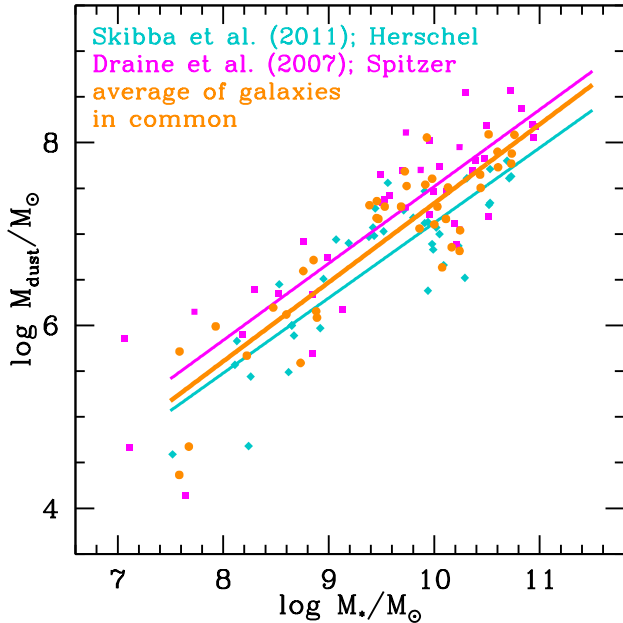


**Figure 4.** Dust masses versus stellar mass from a sample of forty star-forming galaxies, as measured by Skibba et al. (2011) (cyan) and Draine et al. (2007) (pink), and the average of the two samples (orange).

that these longer wavelengths are necessary to fully constrain the mass of *cold* dust (see § 4.2.1 of Skibba et al. 2011 for more discussion).

Finally, it is possible that dust is partially destroyed in the parts of the H II regions where the emission lines used to measure interstellar gas abundances originate. If this were the case, then by separately counting interstellar dust and interstellar gas-phase metals, we might possibly be double counting some of the metals. On the other hand, if it requires shocks from supernovae to destroy dust grains, then the metals in dust should not be fully mixed with the gas in H II regions. Moreover, as ISM gas abundance calibrations typically attempt to correct for depletion of oxygen onto dust (e.g., Kewley & Dopita 2002; Dopita et al. 2013), it is at least commonly assumed that dust is not strongly destroyed in H II regions. For these reasons, we consider it safe to take ISM dust as a distinct reservoir of metals, as long as the dust depletion calibrations are taken into account when considering metals in interstellar gas.

As dust is comprised primarily of heavy elements, we simply adopt

$$M_{Z, \text{dust}} = M_{\text{dust}}. \quad (15)$$

### 3.4. Summary: Metals in Galaxies

The fraction of available metals produced by star-forming  $9.5 \lesssim \log M_{*,0}/M_{\odot} \lesssim 11.5$  galaxies that they retain is a relatively constant  $\sim 20\%$ . The bottom panel of Figure 5 shows  $f_{Z, \text{retain}} \equiv M_{Z, \text{retain}}/M_{Z, \text{made}}$  versus  $\log M_{*,0}$  in bins of  $\log M_{*,0}$ , where  $M_{Z, \text{retain}}(M_{*})$  is the mass of metals in galaxies as stars, interstellar gas, or interstellar dust, i.e.,

$$M_{Z, \text{retain}}(M_{*}) = M_{Z, \star} + M_{Z, \text{ism}} + M_{\text{dust}}. \quad (16)$$

The largest uncertainty in  $f_{Z, \text{retain}}$  owes to uncertainties in the metals produced, specifically from the uncer-

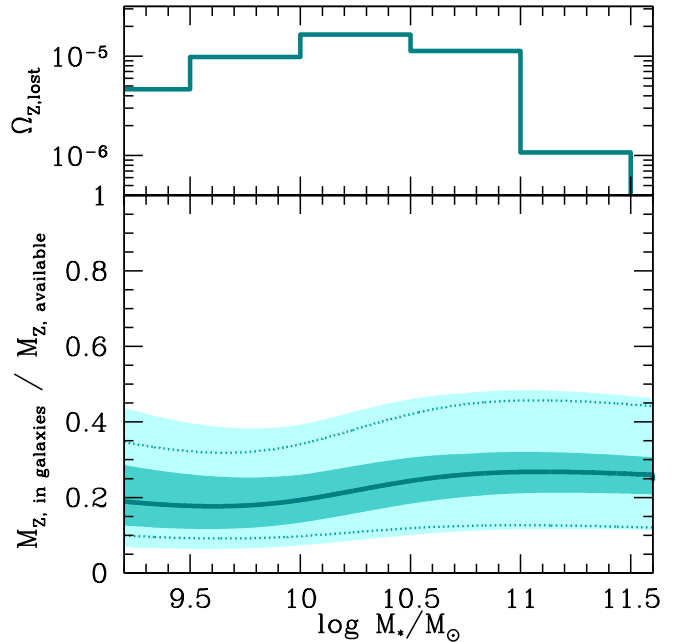


**Figure 5.** *Top:* the cosmic density of metals outside of star-forming galaxies,  $\Omega_{Z, \text{lost}}$ , in bins of the present-day stellar mass of the galaxies where the metals were produced (see equation (17); most of the expelled metals are from  $\sim L^*$  galaxies). *Bottom:* the fraction of metals expelled by SNe and AGB stars that is retained by star-forming galaxies versus galactic stellar mass. The light shaded region shows the total uncertainty, including all sources; the inner dark shaded region, for no uncertainty in the budget, and the dotted lines for no uncertainty in the calibration of the gas-phase metallicities.

tainty in the nucleosynthetic yields ( $y_{z, \text{ii}} = 0.030^{+0.0108}_{-0.0086}$ ), and, to a lesser extent, the Type Ia supernova rate. At lower masses, large gas fractions lead to an uncertainty in the calibration of the gas-phase mass-metallicity relation that becomes nearly as important as the metal production uncertainty (cf. Zahid et al. 2012b). With regards to “how bad is the missing metals problem?” (see § 5), the largest uncertainty still remains the mass of metals to be found.

Regardless of the normalization owing to the nucleosynthetic yields, as  $f_{Z, \text{retain}}$  is relatively constant with respect to stellar mass, the majority of metals that have been expelled from galaxies by  $z = 0$  were produced by stellar populations that are in today’s  $\sim L^*$  galaxies; for star-forming galaxies,  $L^*$  corresponds to  $\log M_{*}/M_{\odot} \sim 10.6$  (Ilbert et al. 2013). The top panel of Figure 5 shows the cosmic density of metals lost from galaxies,

$$\Omega_{Z, \text{lost}} = \frac{1}{\rho_c} \int_{M_{*, \text{min}}}^{M_{*, \text{max}}} M_{Z, \text{lost}}(M_{*}) \frac{dn(M_{*})}{d \log M_{*}} d \log M_{*}, \quad (17)$$

in bins of stellar mass, where  $M_{Z, \text{lost}}(M_{*}) \equiv M_{Z, \text{made}}(M_{*}) - M_{Z, \text{retain}}(M_{*})$ . Despite their shallower potential wells, most of the metals outside of galaxies were not put there by the  $z \sim 0$  dwarf galaxies. However, a substantial fraction of the metals outside of galaxies could have been produced by dwarf galaxies at higher redshifts that were the progenitors of larger present day galaxies (see, e.g., Shen et al. 2012). Specifically, us-

ing the Moustakas et al. (2013) stellar mass function for star-forming galaxies selected from SDSS and GALEX, we find that star-forming galaxies of stellar mass  $10^{8.5}$ – $10^{11.5} M_{\odot}$  have produced metals at a cosmic density of  $\Omega_Z = 5.9 \times 10^{-5}$ , with 78% ( $\Omega_{Z, \text{lost}} = 4.6 \times 10^{-5}$ ) of these metals no longer in galaxies. Broken down by galaxy mass,  $\Omega_{Z, \text{lost}}$  is  $2.6 \times 10^{-5}$  for  $10^{9.5}$ – $10^{10.5} M_{\odot}$  galaxies versus  $7.2 \times 10^{-6}$  for  $M_{\star} = 10^{8.5}$ – $10^{9.5} M_{\odot}$  galaxies and  $1.2 \times 10^{-5}$  for  $10^{10.5}$ – $10^{11.5} M_{\odot}$  galaxies. Analogous to how any given individual star is most likely to be found in an  $L^*$  galaxy, it is a generic result, independent of which form of the stellar mass function is adopted, that the relatively constant fraction of metals expelled by galaxies implies that the bulk of metals outside of galaxies at  $z \sim 0$  were produced by  $\sim L^*$  galaxies.

#### 4. METALS IN THE CIRCUMGALACTIC MEDIUM

If most of the metals produced by galaxies can no longer be found in those galaxies (Figure 5), then the natural place to seek those missing metals is in the immediate vicinity of galaxies, in the circumgalactic medium. As the CGM plays host to complex flows of gas accreting into and ejected from galaxies, we expect it to span a wide range of density, dynamical state, and ionization. We therefore consider here probes of the CGM that trace distinct phases in temperature, density, and ionization state.

COS-Halos addresses the component of CGM metals that can be observed with the suite of multiphase diagnostic UV ions that it was designed around, in the mass range of galaxies selected. As described by Tumlinson et al. (2013), COS-Halos was designed to cover galaxies both with and without active star formation, in the range  $\log M_{\odot}/M_{\odot} \sim 9$ –11.5. The sample was selected to ensure coverage of the key diagnostics of high-ionization gas and metals, and the  $\lambda\lambda 1032, 1038$  doublet of O VI must be observed at  $z > 0.11$  to fall on the COS FUV detectors. At the redshifts of the COS-Halos galaxies,  $0.14 < z < 0.36$ , many other diagnostic ions are also detectable, from the neutral species O I through low ions like C II and Si II and intermediate ions such as C III and Si III. The survey also collected optical data with Keck/HIRES that covered the strong  $\lambda\lambda 2796, 2803$  doublet of Mg II as well as weaker lines of Mg I and Fe II (Werk et al. 2013). With this wide range of diagnostics we can address the metal budget of CGM gas covering a wide range of ionization states. The 28 star forming galaxies in the main COS-Halos sample (Werk et al. 2012) range over  $9.3 < \log M_{\star}/M_{\odot} < 10.8$  with a median  $\log M_{\star}/M_{\odot} = 10.1$ ; these galaxies lie on the mass-metallicity relation (Werk et al. 2012). We therefore consider the COS-Halos results to constrain the metal budget of CGM gas within 150 kpc of galaxies at this typical stellar mass. Though, as we show, there is little dependence of the observed column densities (and thus our inferred CGM metal masses) with stellar mass, the fixed physical radius of 150 kpc corresponds to  $\sim 35$ –110% of the virial radius  $R_{\text{vir}}$  within this stellar mass range (Moster et al. 2010, though see Shull 2014).

As we show in Figure 6, the two predominant phases of the CGM are a patchy, cool ( $\log T \lesssim 5$ ) low-ionization state gas (§ 4.1) and a more highly ionized and uniformly distributed O VI-traced gas (§ 4.2). The much hotter X-ray traced gas (§ 4.3) represents a relatively small contri-

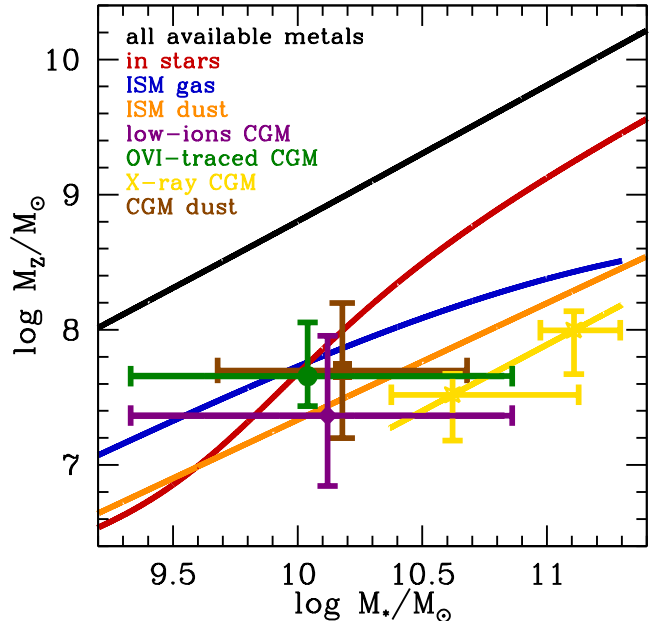


**Figure 6.** Masses of metals in the CGM compared to galaxy components, with low-ionization CGM shown in purple, the O VI-traced CGM shown in green, CGM dust shown in brown, and the X-ray traced CGM shown in yellow.

Component	Fiducial	Minimum	Maximum
Source Components			
Type II SNe	6.8	4.9	10.5
Type Ia SNe	0.76	0.18	2.9
AGB stars	0.45	0.22	0.89
Galactic Components			
Stars	0.72	0.62	0.79
ISM gas	0.81	0.48	1.1
ISM dust	0.26	0.16	0.40
Circumgalactic Components			
Low-ions CGM	0.23	0.069	0.89
O VI-traced CGM	0.46	0.28	1.1
CGM dust	0.50	0.16	1.16

**Table 2**

Fiducial, minimum, and maximum metal masses for metals made available from supernovae and AGB stars, and in each of the galactic and CGM components we consider here, for a galaxy with a present-day stellar mass of  $10^{10.1} M_{\odot}$  (the median stellar mass of galaxies in the COS-Halos sample). All units are in  $10^8 M_{\odot}$ . We do not quote an X-ray traced CGM mass here as this stellar mass is below that of the Anderson et al. (2013) galaxies.

tribution to the overall metal budget of star-forming galaxies. There is, however, a significant mass of metals in circumgalactic dust (§ 4.4). Table 2 shows the fiducial, minimum, and maximum masses at the median COS-Halos galaxy stellar mass of  $10^{10.1} M_{\odot}$ .

##### 4.1. The Low-Ionization Circumgalactic Medium

The mass of metals in the circumgalactic medium in a low-ionization state is

$$M_{Z, \text{lowions}} = \int 2\pi R_{\perp} \Sigma_{Z, \text{lowions}}(R_{\perp}) dR_{\perp}, \quad (18)$$

where the mass surface density of metals  $\Sigma_Z$  is

$$\Sigma_{Z, \text{lowions}} = (\text{Si}/Z)_{\odot} \times m_{\text{Si}} N_{\text{Si}}, \quad (19)$$

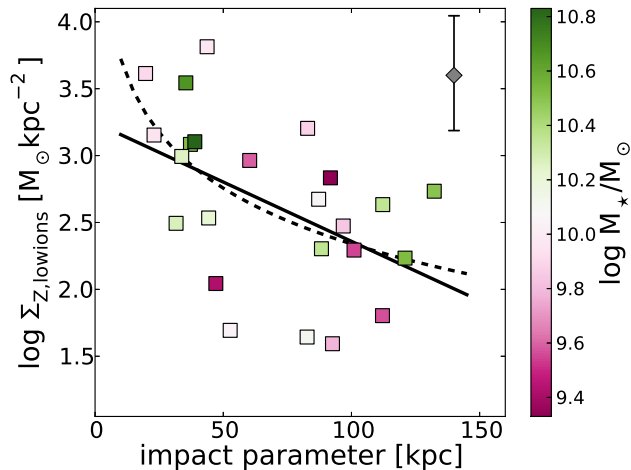


**Figure 7.** The surface density of low-ionization metals as a function of impact parameter and stellar mass; we find no evidence of a strong dependence of  $\Sigma_Z$  on stellar mass. The grey point in the upper-right corner shows the typical uncertainty in the low-ionization metal surface density. The solid and dashed lines are fits to  $\Sigma_Z(R_\perp)$  given in Equation (20) and (21), respectively. These fits are subsequently used in Equation (18) to calculate the low-ionization CGM metal mass.

where  $(\text{Si}/Z)_\odot = 0.04553$  is the Solar mass fraction of metals in silicon (assuming  $12 + \log(\text{Si}/\text{H}) = 7.53$ , Lodders et al. 2009),  $m_{\text{Si}} = 28.0855m_p$  is the mass of a silicon atom, and  $N_{\text{Si}}$  is the ionization-corrected column density of silicon along the line of sight. We integrate Equation (18) over the impact parameter range observed by COS-Halos, from 10 to 150 kpc. We summarize here how the silicon column density  $N_{\text{Si}}$  is derived, with further detail in Werk et al. (in preparation).

For each absorber, we vary the ionization parameter ( $\log U$ ) and the metallicity to search for CLOUDY (v08.00, last described by Ferland et al. 2013) models that are consistent with the column densities of the H I and metal ions determined from the observed UV spectra. We assume the gas is photo-ionized, and thus with temperatures of  $\sim 10^4$  K, which is consistent with the Doppler broadening of the line profiles. The ionization parameter is less susceptible to uncertainties in the H I column density than the gas metallicity, making our measurement of the total metal column density not very sensitive to saturation in the H I lines, which is common in the COS-Halos sample (Tumlinson et al. 2013). This is mostly because we can independently constrain  $\log U$  from the CLOUDY models based on several different ionization states of the same element and the detection of a number of different metal lines of various ionization states (e.g., C II, C III, and C IV; Si II, Si III, and Si IV; N II and N III; Mg I and Mg II). The “intermediate ions”, such as C IV and Si IV, kinematically trace the low-ions, and their column densities are generally well-described by the CLOUDY models. In obtaining the total metal column along an individual sightline, we simply apply an ionization correction to the observed ion column density (e.g.,  $\log N_{\text{SiIII}}$  to  $\log N_{\text{Si}}$ ) based on our CLOUDY analysis; in the few cases lacking robust measurements of silicon lines, we instead use carbon as a proxy for all metals. We then assume relative Solar abundance ratios to derive the total metal surface density (Equation 19). In cases for which we have observed more than two dif-

ferent ionization states for a single element, and more than one element, the uncertainty in the ionization correction along the individual sightline is low,  $< 0.2$  dex. In cases for which we have only a single metal ion, or multiple metals of similar ionization states, the uncertainty in  $\log U$  can be over one dex. The typical uncertainty in the ionization correction leads to an uncertainty in the low-ionization metal surface density of  $\pm 0.42$  dex, as shown in the upper-right corner of Figure 7. In general, our derived temperatures, metallicities, ionization corrections, and subsequently inferred gas masses, are consistent with those found in similar studies using ionization diagnostics to infer CGM physical conditions. (e.g., Stocke et al. 2013).

Figure 7 shows  $\Sigma_{Z,\text{lowions}}$  as a function of impact parameter and stellar mass<sup>17</sup> for the star-forming galaxies in the COS-Halos sample. The surface density profile is well-described by

$$\log \frac{\Sigma_{Z,\text{lowions}}}{M_\odot \text{ kpc}^{-2}} = 3.25 - 0.0089 \left( \frac{R_\perp}{\text{kpc}} \right) \quad (20)$$

and

$$\log \frac{\Sigma_{Z,\text{lowions}}}{M_\odot \text{ kpc}^{-2}} = 5.11 \left( \frac{R_\perp}{\text{kpc}} \right)^{-1.38}; \quad (21)$$

the differences in the CGM metal mass derived from either of these fits is negligible. With the current data, there is no measurably significant dependence of surface density on the stellar mass of the central galaxy. We, therefore, derive a low-ionization CGM metal mass of

$$\log M_{Z,\text{lowions}}/M_\odot = 7.36 \pm 0.14^{\text{(stat)}} +_{-0.38}^{+0.45\text{(sys)}}, \quad (22)$$

where the statistical uncertainty is derived by bootstrapping over the data sample and re-fitting the surface density profile and the systematic uncertainty owes to the uncertainties in the ionization corrections.

If other galaxies have high velocity clouds (HVCs; Muller et al. 1963), such as those seen around the Milky Way, this gas would be a (small) subset of the low-ionization CGM detected by COS-Halos. These discrete gas clouds lie mostly within  $\sim 10$  kpc of the Galactic plane (Wakker et al. 2007, 2008; Thom et al. 2008; Hsu et al. 2011). Though their covering fraction on the sky is high,  $\sim 18$ –67% (depending on their H I column density, Sembach et al. 2000; Lockman et al. 2002; Shull et al. 2009; Lehner & Howk 2011; Shull et al. 2011; Lehner et al. 2012; Putman et al. 2012), their total mass is only  $M_{\text{hvc}} \sim 10^8 M_\odot$  (Shull et al. 2009; Putman et al. 2012, though see also Lehner & Howk 2011 for a slightly higher estimated mass of ionized HVCs). Taking this mass with a fiducial  $Z_{\text{hvc}} = 0.2Z_\odot$  and Solar abundance ratios, we find a mass of metals in this high-velocity circumgalactic component of  $M_{Z,\text{hvc}} \sim 3 \times 10^5 M_\odot$ , which is small relative to other circumgalactic (or galactic) components of  $L^*$  galaxies.

#### 4.2. The High-Ionization Circumgalactic Medium

Tumlinson et al. (2011) found  $N_{\text{OVI}} \sim 10^{14.5} \text{ cm}^{-2}$  around star-forming galaxies out to impact parameters

<sup>17</sup> We have converted the Werk et al. stellar masses to a Chabrier IMF from a Salpeter IMF.

of 150 kpc (as shown in the top panels of Figure 8). For the most part, this O VI absorption is kinematically distinct from the low-ionization gas, and its high column density is inconsistent with the O VI-traced gas being in the same ionization state, temperature, and density as the low-ionization gas (§ 4.1; Werk et al. in preparation); we therefore consider the material traced by this O VI absorption as an additional reservoir of metals.

Using a similar method to the one we used in § 4.1, Tumlinson et al. (2011) found an O VI-traced oxygen mass of  $M_{\text{oxy, OVI}} \geq 1.2 \times 10^7 M_{\odot}$ . This estimate is a direct numerical integration over column densities and surveyed volumes, and assumes the maximum O VI ionization fraction  $f_{\text{OVI}} = 0.2$  achieved in photo- and/or collisional ionization to set a lower limit on the column density and mass of total oxygen. In this simple integration,  $M_{\text{oxy, OVI}} \propto f_{\text{OVI}}^{-1}$ , so the total oxygen mass can increase substantially above this conservative minimum if the detected O VI is not at its optimal conditions for ionization. In particular, the maximum O VI ionization fraction  $f_{\text{OVI}} = 0.2$  occurs at  $T \sim 10^{5.5}$  K, where cooling times are short and therefore such a massive reservoir of gas is presumably short-lived.

To impose a conservative limit on the CGM oxygen mass, Tumlinson et al. (2011) did not consider oxygen away from its optimal ionization fraction in O VI, and did not consider gas outside the 150 kpc region of the COS-Halos survey. To assess how much more oxygen mass there could be out to  $R_{\text{vir}}$  than the conservative minimum, we consider simple 1-D halo models wherein we take into account not only the overall level of O VI absorption, but also its profile as seen through projection. In these descriptive models, we take the density profile of the CGM to be a power-law with a slope  $\alpha$ , normalized to an overdensity  $\delta_0$  at a radius  $R_0 = 300$  kpc, i.e.,

$$\delta = \delta_0 \left( \frac{R}{300 \text{ kpc}} \right)^{\alpha}, \quad (23)$$

with the inner 10 kpc sphere (which would not be considered part of a halo) set to zero density to prevent numerical divergence. The O VI temperature is set to a constant  $T$ . This 1-D model is then projected into a 3-D spherical distribution. Mock sightlines are then passed through this medium at a fixed projected separation (impact parameter) and column densities of O VI are obtained via line integrals along the sightline. The models assume that the diffuse gaseous medium is exposed to the Haardt & Madau (2001) radiation background, and includes a component for collisional ionization equilibrium at the parametric temperature. These models were also used in Tumlinson et al. (2013) to assess the total H I masses in galaxy halos from the COS-Halos H I survey.

The primary parameters in this model are the exponent of the density power law  $\alpha$ , the density normalization at  $R_0 = 300$  kpc,  $\delta_0$ , and the gas temperature  $T$ . To estimate the amount of O VI, and from that the oxygen masses in the model halos, we produce grids of models with  $T = 10^4$ – $10^6$  K and  $\alpha = -1$  or  $-2$ . We then use a simple likelihood analysis to find the set of parameters that best match the O VI detections for the COS-Halos star-forming sample. The allowable model profiles for  $\alpha = -1$  and  $-2$  appear in the top panels of Figure 8; the

bottom panels show the contours of total oxygen mass in the  $\delta_0$  v.  $T$  parameter space. Here we see that the low-temperature ( $T \sim 10^5$  K) solution exists for both values of  $\alpha$  and gives a total mass to 150 kpc of 3 to  $5 \times 10^7 M_{\odot}$ , a few times higher than the conservative minimum.

The main controlling parameter is the power-law slope of the density profile, for which we have no independent constraint; if we take the much shallower profile of  $\alpha = -1$ , then a much more massive ( $M_{\text{oxy, OVI}} \sim 2 \times 10^8 M_{\odot}$ ), higher density ( $\delta_0 \sim 100$ ), hotter ( $T \sim 10^6$  K) solution becomes possible. The choice of  $R_0$  affects the best-fit overdensity, but does not have a large impact on the implied mass within 150 kpc. For the mass of oxygen traced by O VI within a cylinder of radius 150 kpc, we therefore take

$$M_{\text{oxy, OVI}} = \begin{cases} 1.2 \times 10^7 M_{\odot}, & \text{minimum,} \\ 2 \times 10^7 M_{\odot}, & \text{fiducial, and} \\ 5 \times 10^7 M_{\odot}, & \text{maximum.} \end{cases} \quad (24)$$

To derive a metal mass, we assume a Solar oxygen-to-metals ratio of 44%, as done for the ISM in § 3.2.2. As with the low-ionization metals, we note that we do not see a dependence of  $N_{\text{OVI}}$  on stellar mass within the 1.5 dex mass range in  $M_{\star}$  spanned by our sample.

It is possible that the O VI-traced gas is in a transient phase, potentially cooling out of a hotter reservoir or “boiling off” of cooler clouds; either way, one would expect for the reservoir the O VI-traced gas is transitioning out of to be more massive than the O VI-traced gas itself. This simple picture, however, is at odds with the relatively lower masses of other CGM components, unless, e.g., the “hotter” component is  $< 5.8 \times 10^6$  K (i.e., 0.5 keV) and therefore not readily detected in the X-rays. By design, our “O VI-traced” mass does not address such a “hidden” reservoir, which would only add to the CGM metal mass budget.

#### 4.3. The X-Ray Traced Circumgalactic Medium

Anderson et al. (2013) used stacked ROSAT images to place constraints on the X-ray luminosity and thus hot ( $T \gtrsim 6 \times 10^6$  K) CGM gas mass out to  $\sim 50$  kpc. They find that late-type galaxies with  $L_K = 1.35^{+0.72}_{-0.36} \times 10^{11} L_{\odot}$  have a hot X-ray halo with gas mass  $M_{\text{hotgas}} = 3.6^{+0.8}_{-1.1} \times 10^9 M_{\odot}$  for a metallicity of  $0.3 Z_{\odot}$ ; as their systematic uncertainty in the gas mass scales roughly linearly with the assumed metallicity, we adopt  $0.3 Z_{\odot}$ . For fainter late-type galaxies, with  $L_K = 4.4^{+9.7}_{-1.9} \times 10^{10} L_{\odot}$ , extended X-ray emission is not robustly detected in the stacked images, although they give an estimate of the hot CGM mass of  $M_{\text{hotgas}} = 1.2^{+0.5}_{-0.6} \times 10^9 M_{\odot}$ . Furthermore, Anderson et al. argue that there cannot be a massive reservoir of hot gas at galactocentric radii of  $\gtrsim 50$  kpc. These hot CGM masses are consistent with other probes of hot gaseous halos around  $\sim L^*$  galaxies, including the dispersion measure toward pulsars in the Large Magellanic Cloud, the pressure confinement of HVCs in the Milky Way’s halo, the (lack of) O VII absorption in the halos of other galaxies, and X-ray surface brightness limits from individual galaxies (Anderson & Bregman 2010, though see also Fang et al. 2013). Likewise, Yao et al. (2010) did not detect X-ray absorption from a plethora of metal lines in stacked Chandra grating spectra in 12

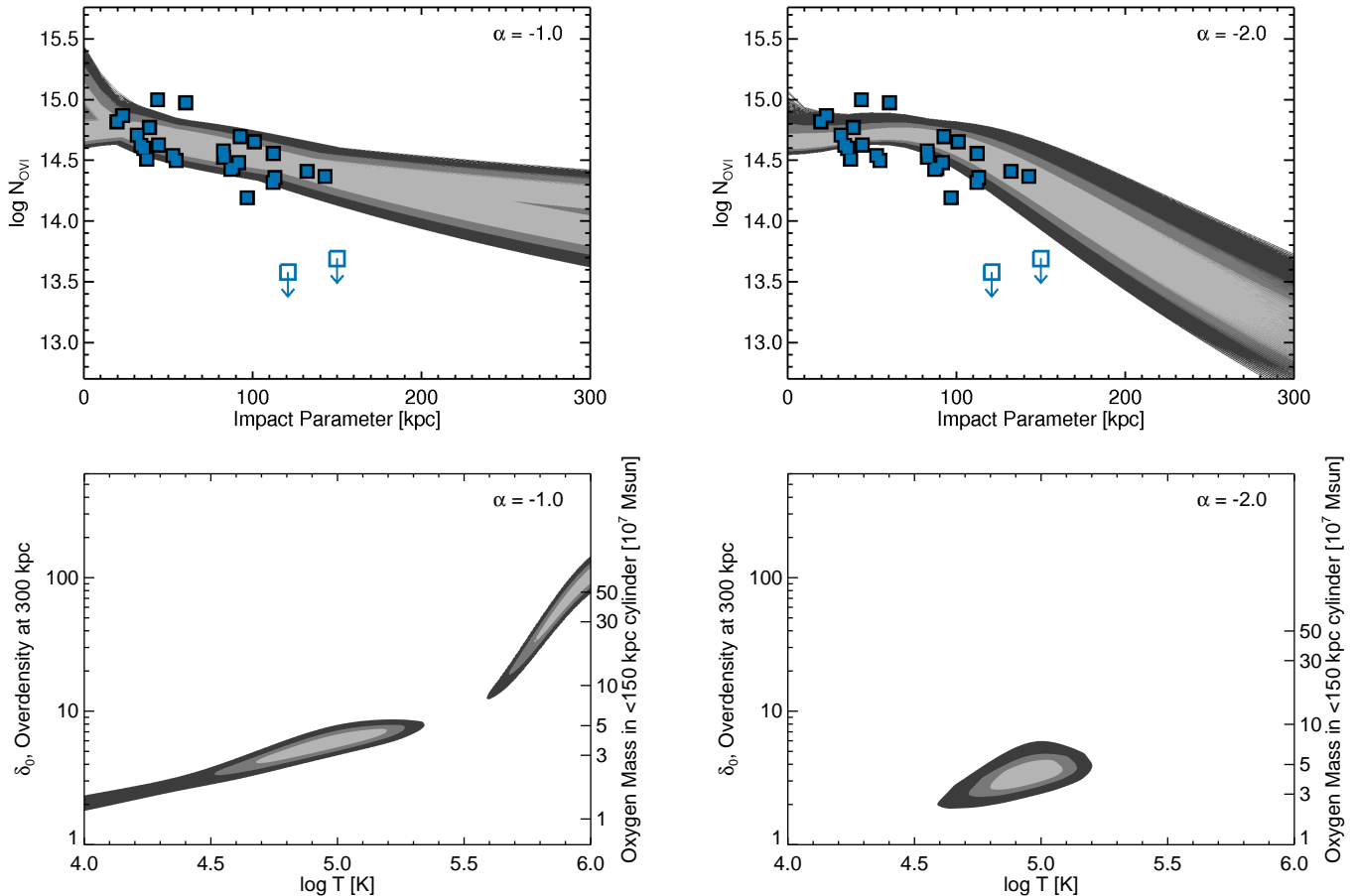


**Figure 8.** Top panels: O VI column density profiles from simple halo models showing the range of profiles in agreement with the data at 1, 2, and 3  $\sigma$  confidence, with  $\alpha = -1$  (left column) and  $-2$  (right column). Detections of O VI around the COS-Halos star-forming galaxies are overlaid in blue. Higher impact parameter data from Prochaska et al. (2011) prefer the  $\alpha = -2$  model. Bottom panels: Corresponding temperatures and overdensities for the simple halo models. The oxygen masses in cylinders of radius 150 kpc are degenerate with the density normalization.

CGM sightlines, strongly suggesting that hot  $Z_{\odot}$  gas cannot fill a typical CGM volume. We stress that this picture—in which there is a relatively small amount of material in a coronal X-ray traced phase—is dramatically different from what is expected for galaxies living in more massive halos with higher virial temperatures, especially rich galaxy clusters.

Following Anderson et al. (2013), in Figure 6, we show the mass of metals in a hot phase extrapolated out to 150 kpc around late-type galaxies to be

$$\log M_{\text{hotcg},Z}/M_{\odot} = 0.98(\log M_{*,0}/M_{\odot} - 11) + 7.89, \quad (25)$$

adopting a  $K$ -band mass-to-light ratio of  $M_{*}/L_K = 0.95 M_{\odot}/L_{\odot}$  (Bell et al. 2003). This represents the fiducial Anderson et al. (2013) values increased by a factor of 6 to account for out to 150 kpc. This extrapolation is uncertain as it depends on the unknown slope of the hot halo profile (Kaufmann et al. 2009; Feldmann et al. 2013); we, therefore, let this mass ratio extrapolation factor vary from 3 to 8.<sup>18</sup> Finally, we note that the stellar mass range of the galaxies in the Anderson et al. (2013) sample is  $\sim 1$  dex higher than those in the COS-Halos

sample.

#### 4.4. Dust outside of galaxies

Measuring the systematic reddening of background quasars relative to their projected distance from foreground galaxies from SDSS, Ménard et al. (2010) derived a CGM dust mass of  $M_{\text{dust}}^{\text{cgm}} \simeq 5 \times 10^7 M_{\odot}$  for  $20h^{-1}\text{kpc} < r_{\text{eff}} < r_{\text{vir}}$  around  $\sim 0.5L^*$  galaxies. This mass is consistent with the dust expected to be associated with the level of Mg II absorption seen in the COS-Halos sample (Ménard et al. 2008; Ménard & Fukugita 2012; Werk et al. 2013). Though this dust mass is calculated for out to  $R_{\text{vir}}$ , as opposed to the 150 kpc we adopt for the other CGM reservoirs, more recent results are showing that CGM dust is primarily confined to within 150 kpc of galaxies (Peek et al., in preparation). We adopt  $\log M_{\text{dust}}^{\text{cgm}}/M_{\odot} = 7.7 \pm 0.5$  for a stellar mass range of  $9.7 \leq \log M_{*}/M_{\odot} \leq 10.7$ .

The Ménard et al. average galaxy redshift is  $\simeq 0.36$ , so by  $z = 0$  these dust masses could grow somewhat larger. However, this typical redshift is only slightly above that of the COS-Halos median redshift. Finally, we note that this  $M_{\text{dust}}^{\text{cgm}}$  combined with the COS-Halos results (§§4.1–4.2) implies that  $\sim 42\%$  of CGM metals by mass are in a solid phase, which is remarkably close

<sup>18</sup> We thank M. Anderson for calculating the extent of this extrapolation to 150 kpc.

to the simulation results of [Zu et al. \(2011\)](#), who found that a dust mass fraction of 0.39 was required to reproduce [Ménard et al. \(2010\)](#) results in a momentum-driven wind model that also reproduces observed galaxy properties and intergalactic enrichment. (Intriguingly, this dust mass ratio of 0.42 is slightly higher than the interstellar ratio of  $\sim 0.3$  in the same  $M_*$  range.)

### 5. HOW BAD IS THE MISSING METALS PROBLEM?

We address here the so-called “missing metals problem”: does the sum total of metals found in the reservoirs explored here, i.e., those inside galaxies (§3) and those in the observed circumgalactic medium (§4), fully account for the available budget of metals produced (§2)? The answer to this question largely depends on the quantity of metals that galaxies have produced. As shown in Figure 5, the uncertainties in the nucleosynthetic yields are large enough that they can easily dominate this question: we must know how many metals we are looking for before we can determine whether or not they have all been found. For the discussion here we will consider as the available metal budget just the fiducial values discussed in §2, with the caveat that more accurate yields could easily change our conclusions one way or the other.

In Figure 9, we show the fraction of metals that were ever produced and subsequently expelled by supernovae and stellar winds as currently observed in each of the components in each of the three galactic (stars, interstellar gas and dust; §3) and the four major CGM (low-ionization, O VI-traced, dust, X-ray traced, each out to 150 kpc; §4) components we consider. That is, we produce the left panel of Figure 9 by dividing the fiducial values in Figure 6 by the fiducial “available” metals line. The right panel plots the same information, but as cumulative fractions. Only a few percent of the available metals are in interstellar dust,  $\sim 5\text{--}10\%$  are in interstellar gas, and, in the galactic stellar mass range that we consider, the massive galaxies have more metals trapped in stars than the smaller galaxies have in the ISM. It is also immediately obvious from Figure 9 that at  $\log M_*/M_\odot \lesssim 10$  the observed CGM could dominate the metal budget, though at higher masses it is still comparable to the metals found in galaxies. The sharp fractional increase in the O VI-traced and low-ionization CGM stems from the fact that we are dividing constant CGM masses by a steeply changing mass of available metals; we caution that though our data does not indicate a dependence of CGM metal mass within 150 kpc on stellar mass, this is both a fixed *physical* radius, and we are limited by relatively small numbers.

In the fiducial case, we find that at about a Milky Way mass, roughly 40% of all available metals are easily accounted for when including measurements of the CGM out to 150 kpc. Figure 10 shows the “pessimistic” and “optimistic” cases for all metals, i.e., where we set the masses of each of the individual components to either their minima or maxima, respectively, while keeping the available budget at its fiducial value. Here, we see that at the median mass of the COS-Halos sample,  $\log M_*/M_\odot \sim 10.1$ , the uncertainties imply that we do not account for between 25 to 70 percent of metals. Within galaxies, the largest source of this uncertainty is from the uncertainty in the gas-phase metallicities, especially at low  $M_*$ .

Reducing the uncertainty in the interstellar abundance calibrations would help constrain the fraction of metals remaining in galaxies; it is possible that new emission line diagnostics adopting a  $\kappa$ -distribution for the electron energies could resolve some of the systematic uncertainties currently plaguing this field, leading to smaller uncertainties in the near future ([Nicholls et al. 2012](#); [Dopita et al. 2013](#)). Resolved H II-region metallicity mapping, such as the upcoming Mapping Nearby Galaxies at APO (MaNGA) program with SDSS-IV, combined with resolved gas maps could also reduce the need to make strong assumptions about how well the ISM is mixed.

With regards to the UV-traced CGM, until we can resolve this gas in emission and accurately map its morphology and extent for individual galaxy halos, absorption line studies are the only way to detect and characterize this massive reservoir. Given the apparent patchiness of the low-ionization CGM, with only  $\sim 40$  sightlines, the COS-Halos sample is not large enough to detect trends in CGM properties with respect to galaxy mass. In particular, it is unclear with the absorption line approach how much of the large scatter in column density (Figure 7) is galaxy-to-galaxy variation as opposed to genuine CGM substructure. Fortunately, the metallic CGM is easier to quantify than the baryonic CGM; as most of the observable transitions are from metal ions probing a large temperature range, no metallicity correction is needed, and a large hidden reservoir of predominantly ionized metal-poor gas will affect the metal census less than the baryonic one.

For the other CGM components, our inventory relies on a statistical measure of the CGM dust mass, but it is possible for the same kind of reddening studies to target different masses of foreground galaxies ([Peek et al.](#), in preparation). Likewise, the [Ménard et al. \(2010\)](#) analysis does not constrain the chemical makeup of the circumgalactic dust (see further discussion in the Appendix). Finally, we note that we currently must assume a metallicity of the X-ray traced CGM component instead of directly measuring a metal mass, but as this component is relatively small around the galaxies that we are considering, the contribution of this uncertainty to the total metal census uncertainty is not large. A larger contributing factor is the uncertainty in the slope of the X-ray profile, especially beyond 150 kpc, as a very flat profile could lead to a total hot halo mass that is several times larger than we quote here ([Kaufmann et al. 2009](#); [Crain et al. 2013](#); [Feldmann et al. 2013](#); [Anderson et al. 2013](#); [Fang et al. 2013](#)).

As metals (e.g., O VI) are observed at impact parameters beyond 150 kpc ([Prochaska et al. 2011](#); [Stoche et al. 2013](#)), we do not expect that even in the most optimistic scenario for our current accounting to have found all of the metals. For example, an extrapolation of the O VI column densities following the  $\alpha = -2$  profile in Figure 8 to an impact parameter of 300 kpc is consistent with the O VI observations from [Prochaska et al. \(2011\)](#). Despite an increase in volume of a factor of eight, extrapolating this profile from 150 to 300 kpc would only roughly double the (spherical) O VI-traced CGM metal mass.

## 6. CONCLUSIONS AND DISCUSSION

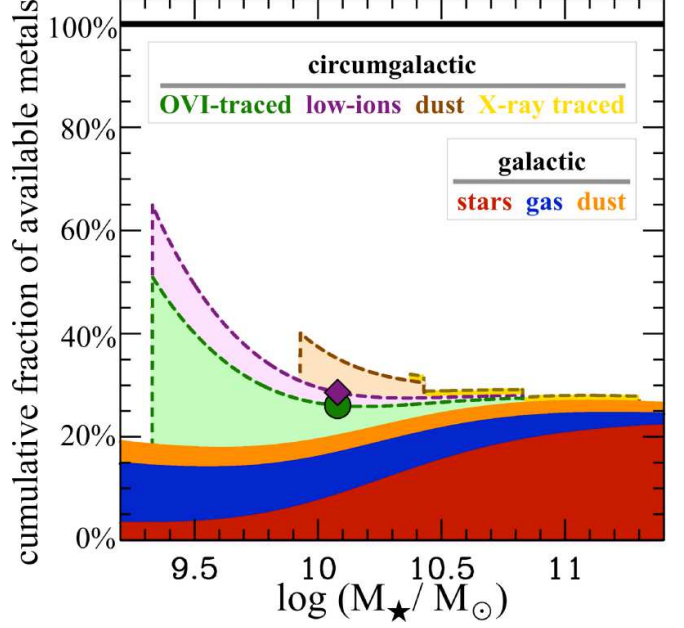
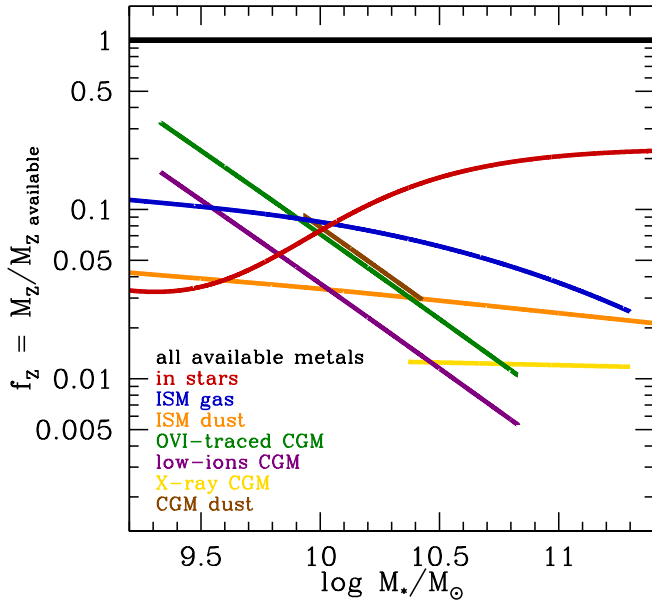


**Figure 9.** Fractions (*left*) and cumulative fractions (*right*) of available metals in various components as a function of stellar mass. Note that the CGM masses are within a fixed *physical* radius of 150 kpc—and thus sampling different fractions of the virial radius with respect to stellar mass.

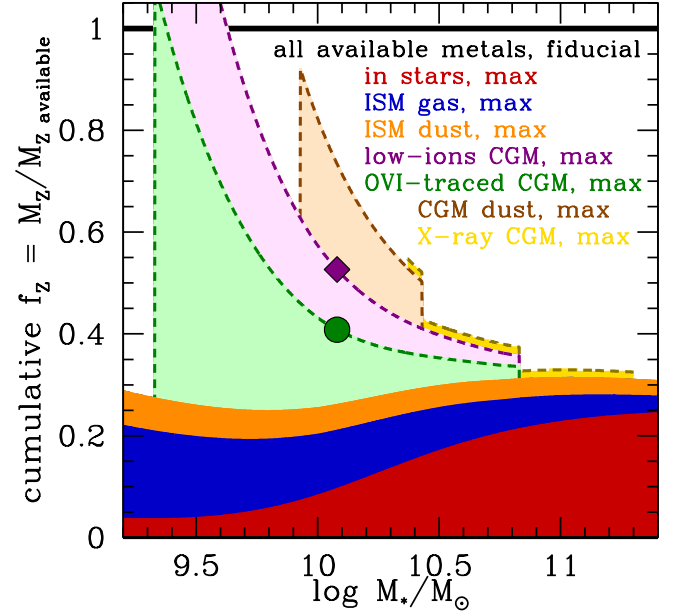
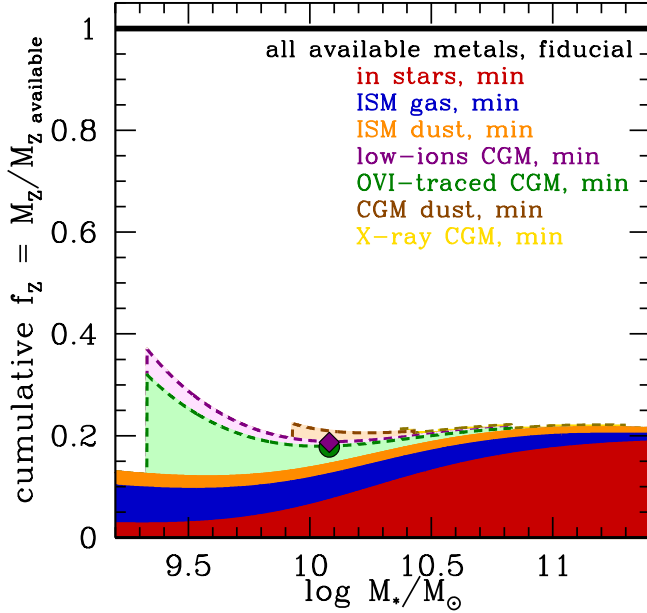


**Figure 10.** Pessimistic (*left*) and optimistic (*right*) cumulative metal fractions. In the “pessimistic” case, we set the values of the mass of metals in each galactic and circumgalactic component to the minimum value allowed within our uncertainties; in the “optimistic” case, we take the maximum allowed values. In both cases, we compare to the fiducial values for available metals.

We have compiled an accounting of metals in and around star-forming  $\sim L^*$  galaxies at  $z \sim 0$  and compared this census to the available budget of heavy elements produced and expelled by supernovae and stellar winds. We find:

1. Galaxies with stellar masses  $10^9$ – $10^{11.5} M_\odot$  retain in their stars, ISM, and dust a roughly constant  $\sim 20$ – $25\%$  of the metals they have produced. Thus, the bulk of metals outside of galaxies at  $z = 0$

were produced by (the precursors to) today’s  $\sim L^*$  galaxies.

2. About half of the metals produced by typical star-forming galaxies can be accounted for by considering the CGM out to  $\sim 150$  kpc when added to the stellar and interstellar components. Most of these circumgalactic metals are in a highly ionized O VI-traced phase or in dust. The low-ionization CGM metal mass is subdominant, though not neg-

ligible. We find the metals in a circumgalactic hot gas component are small compared to ISM contributions, based on the hot gas halo mass estimates of Anderson et al. (2013) with a metallicity of  $0.3Z_{\odot}$ .

3. With the current data, there is no evidence for a steep dependence on galaxy mass in the metal surface density in the CGM (within this stellar mass range). Though the metal surface density does decline with impact parameter, the sightline-to-sightline variation for the low-ionization CGM is large, suggesting that the low-ionization CGM is patchy (cf. Werk et al. 2013).
4. The largest source of uncertainty in the “missing metals problem” is from the uncertainties in the nucleosynthetic yields; to know what fraction of metals we have found, we must first know how many metals we are seeking.

There are two important improvements that should be made to this  $z \sim 0$  metal accounting: finding the “missing” metals, and expanding the census to other galaxy populations. Within galaxies, unaccounted-for metals could be in a warm, ionized component of the ISM (i.e., the WIM, § 3.2). In the CGM, metals could be hiding in a hotter reservoir from which the O VI-traced gas might be cooling, provided it is still too cool to be detected in X-ray emission (i.e.,  $T \lesssim 1\text{--}5 \times 10^6$  K). Constraints on such a reservoir could be placed by observing the CGM in higher ionization transitions such as Ne VIII or Mg X (Savage et al. 2011; Narayanan et al. 2011; Ford et al. 2013). Finally, as discussed in § 5, our current inventory is by construction missing the metals at impact parameters  $> 150$  kpc (Prochaska et al. 2011). While the UV-traced CGM could be mapped using QSO absorption lines as done in the COS-Halos survey, a next-generation X-ray telescope such as the International X-ray Observatory (IXO; Bookbinder et al. 2012) would be required to detect, e.g., low-column density O VII expected to be found at high impact parameters (Anderson et al. 2013; Hummels et al. 2013).

The two main galaxy populations lacking from our inventory are passive galaxies and dwarf galaxies. Gallazzi et al. (2008) found that as much as  $\sim 40\%$  of the metals produced by bulge-dominated galaxies could be currently residing in their stars. The circumgalactic metal content of passive galaxies with  $\log M_{\star}/M_{\odot} \sim 10.5$  to 11 can begin to be addressed with COS-Halos. Intriguingly, while the properties of the low-ionization state absorbers around the passive galaxies are statistically similar to those around star-forming galaxies (Thom et al. 2012; Werk et al. 2013), passive galaxies have extremely little O VI in their halos (Tumlinson et al. 2011). More massive galaxies than those probed by the COS-Halos survey are also expected to reside in halos with higher virial temperatures, and so it is also reasonable to expect that more massive passive galaxies have a larger fraction of their circumgalactic gas traced by X-ray emitting rather than UV-absorbing gas. On the other hand, the star-formation histories and IMFs (and IMF histories), and thus available metal budgets, are somewhat more difficult to constrain for passive galaxies. Likewise, while

their dust content should be negligible, passive galaxies do have an interstellar medium. This ISM, though, is generally not cold, and—by definition—not lit up by H II regions, making its metal content difficult to ascertain. It is possible, though, that passive galaxies with low-ionization emission (i.e., LINERS) could have their interstellar metal content probed with analogous methods (Yan & Blanton 2012).

Dwarf galaxies pose a somewhat different and interesting set of obstacles to understanding the eventual fate of their metals. From the results we show here, it is obvious that the uncertainties in the gas masses will be much more relevant for  $M_{\star} < 10^{9.5} M_{\odot}$  galaxies, and, simultaneously, it is less clear to what extent the ISM of dwarf galaxies is mixed, and thus whether or not equation (8) is valid. Moreover, in star forming galaxies, it appears that the dust in dwarf galaxies is higher than the metal mass locked up in stars; as this conclusion is based on very few galaxies, a full census of metals in star-forming dwarf galaxies will require a better understanding of their dust content. Moreover, dwarf galaxies have had more stochastic star formation histories (Weisz et al. 2011) and appear to have larger spread in gas-phase metallicities (Zahid et al. 2012a) than  $\sim L^*$  galaxies. Some of this stochasticity might be attributable to environment, as metallicities (Pasquali et al. 2010, 2012) and star formation (i.e., passive versus star-forming; Geha et al. 2012) properties strongly depend on the degree of isolation. With regards to the CGM of dwarf galaxies, our group has another large *HST* program, COS-Dwarfs (PID 12248, 129 HST orbits, PI: J. Tumlinson), designed to map the CGM of  $8 \lesssim \log M_{\star}/M_{\odot} \lesssim 9.5$  galaxies out to  $\sim 150$  kpc in H I, C II, C IV, Si I, Si II, Si IV, and other species, with which we will address these questions.

We thank M. Shull for a thoughtful, detailed, and rapid referee’s report. We are grateful to M. Anderson, K. Barger, E. Bell, R. Bordoloi, M. Childress, M. Dopita, A. B. Ford, A. Fox, E. Jenkins, J. C. Howk, J. Kalirai, N. Lehner, S. Mathur, B. Ménard, S. Oey, J. E. G. Peek, R. S. Somerville, C. Thom, and S. Trager for useful and interesting conversations that have improved this paper. Support for program GO11598 was provided by NASA through a grant from the Space Telescope Science Institute, which is operated by the Association of Universities for Research in Astronomy, Inc., under NASA contract NAS 5-26555. MSP acknowledges support from the Southern California Center for Galaxy Evolution, a multi-campus research program funded by the University of California Office of Research. This research has made extensive use of NASA’s Astrophysics Data System.

## REFERENCES

- Anderson, M. E. & Bregman, J. N. 2010, *ApJ*, 714, 320  
 Anderson, M. E., Bregman, J. N., & Dai, X. 2013, *ApJ*, 762, 106  
 Arrigoni, M. 2010, PhD thesis, University of Groningen  
 Arrigoni, M., Trager, S. C., Somerville, R. S., & Gibson, B. K. 2010, *MNRAS*, 402, 173  
 Asplund, M., Grevesse, N., Sauval, A. J., & Scott, P. 2009, *ARA&A*, 47, 481  
 Auger, M. W., Treu, T., Gavazzi, R., Bolton, A. S., Koopmans, L. V. E., & Marshall, P. J. 2010, *ApJ*, 721, L163  
 Bahcall, J. N., Basu, S., Pinsonneault, M., & Serenelli, A. M. 2005, *ApJ*, 618, 1049

- Bell, E. F., McIntosh, D. H., Katz, N., & Weinberg, M. D. 2003, *ApJS*, 149, 289
- Bernardi, M., Shankar, F., Hyde, J. B., Mei, S., Marulli, F., & Sheth, R. K. 2010, *MNRAS*, 436
- Berry, M., Somerville, R. S., Haas, M. R., Gawiser, E., Maller, A., Popping, G., & Trager, S. C. 2013, arXiv:1308.2598
- Bookbinder, J. A., Smith, R. K., Bandler, S., Garcia, M., Hornschemeier, A., Petre, R., & Ptak, A. 2012, in *Society of Photo-Optical Instrumentation Engineers (SPIE) Conference Series*, Vol. 8443, Society of Photo-Optical Instrumentation Engineers (SPIE) Conference Series
- Booth, C. M., Schaye, J., Delgado, J. D., & Dalla Vecchia, C. 2012, *MNRAS*, 420, 1053
- Bouché, N., Lehnert, M. D., Aguirre, A., Péroux, C., & Bergeron, J. 2007, *MNRAS*, 378, 525
- Bouché, N., Lehnert, M. D., & Péroux, C. 2005, *MNRAS*, 364, 319
- , 2006, *MNRAS*, 367, L16
- Brewer, B. J., Dutton, A. A., Treu, T., Auger, M. W., Marshall, P. J., Barnabè, M., Bolton, A. S., Koo, D. C., & Koopmans, L. V. E. 2012, *MNRAS*, 422, 3574
- Bruzual, G. & Charlot, S. 2003, *MNRAS*, 344, 1000
- Caffau, E., Ludwig, H.-G., Steffen, M., Freytag, B., & Bonifacio, P. 2011, *Sol. Phys.*, 268, 255
- Cartledge, S. I. B., Lauroesch, J. T., Meyer, D. M., & Sofia, U. J. 2004, *ApJ*, 613, 1037
- Chabrier, G. 2003a, *PASP*, 115, 763
- , 2003b, *ApJ*, 586, L133
- Chieffi, A. & Limongi, M. 2004, *ApJ*, 608, 405
- Conroy, C., Dutton, A. A., Graves, G. J., Mendel, J. T., & van Dokkum, P. G. 2013, *ApJ*, 776, L26
- Conroy, C. & van Dokkum, P. G. 2012, *ApJ*, 760, 71
- Crain, R. A., McCarthy, I. G., Schaye, J., Theuns, T., & Frenk, C. S. 2013, *MNRAS*, 432, 3005
- da Cunha, E., Charlot, S., & Elbaz, D. 2008, *MNRAS*, 388, 1595
- Dalcanton, J. J. 2007, *ApJ*, 658, 941
- Davé, R., Finlator, K., & Oppenheimer, B. D. 2011, *MNRAS*, 416, 1354
- Dayal, P., Ferrara, A., & Dunlop, J. S. 2013, *MNRAS*, 430, 2891
- Delahaye, F. & Pinsonneault, M. H. 2006, *ApJ*, 649, 529
- Dopita, M. A., Sutherland, R. S., Nicholls, D. C., Kewley, L. J., & Vogt, F. P. A. 2013, *ApJS*, 208, 10
- Draine, B. T. 2003, *ARA&A*, 41, 241
- , 2011, *Physics of the Interstellar and Intergalactic Medium*
- Draine, B. T., Dale, D. A., Bendo, G., Gordon, K. D., Smith, J. D. T., Armus, L., Engelbracht, C. W., Helou, G., Kennicutt, Jr., R. C., Li, A., Roussel, H., Walter, F., Calzetti, D., Moustakas, J., Murphy, E. J., Rieke, G. H., Bot, C., Hollenbach, D. J., Sheth, K., & Teplitz, H. I. 2007, *ApJ*, 663, 866
- Draine, B. T. & Fraise, A. A. 2009, *ApJ*, 696, 1
- Dutton, A. A., Macciò, A. V., Mendel, J. T., & Simard, L. 2013, *MNRAS*, 432, 2496
- Erb, D. K. 2008, *ApJ*, 674, 151
- Fang, T., Bullock, J., & Boylan-Kolchin, M. 2013, *ApJ*, 762, 20
- Feldmann, R., Hooper, D., & Gnedin, N. Y. 2013, *ApJ*, 763, 21
- Ferland, G. J., Porter, R. L., van Hoof, P. A. M., Williams, R. J. R., Abel, N. P., Lykins, M. L., Shaw, G., Henney, W. J., & Stancil, P. C. 2013, *RMxAA*, 49, 137
- Ferrara, A., Scannapieco, E., & Bergeron, J. 2005, *ApJ*, 634, L37
- Finlator, K. & Davé, R. 2008, *MNRAS*, 385, 2181
- Ford, A. B., Oppenheimer, B. D., Davé, R., Katz, N., Kollmeier, J. A., & Weinberg, D. H. 2013, *MNRAS*, 432, 89
- Fukugita, M., Hogan, C. J., & Peebles, P. J. E. 1998, *ApJ*, 503, 518
- Fukugita, M. & Peebles, P. J. E. 2004, *ApJ*, 616, 643
- Gallazzi, A., Brinchmann, J., Charlot, S., & White, S. D. M. 2008, *MNRAS*, 383, 1439
- Gallazzi, A., Charlot, S., Brinchmann, J., White, S. D. M., & Tremonti, C. A. 2005, *MNRAS*, 362, 41
- Garnett, D. R. 2002, *ApJ*, 581, 1019
- Gavilán, M., Buell, J. F., & Mollá, M. 2005, *A&A*, 432, 861
- Geha, M., Blanton, M. R., Yan, R., & Tinker, J. L. 2012, *ApJ*, 757, 85
- Geha, M., Brown, T. M., Tumlinson, J., Kalirai, J. S., Simon, J. D., Kirby, E. N., VandenBerg, D. A., Muñoz, R. R., Avila, R. J., Guhathakurta, P., & Ferguson, H. C. 2013, *ApJ*, 771, 29
- Gibson, B. K., Loewenstein, M., & Mushotzky, R. F. 1997, *MNRAS*, 290, 623
- Haardt, F. & Madau, P. 2001, in *Clusters of Galaxies and the High Redshift Universe Observed in X-rays*, ed. D. M. Neumann & J. T. V. Tran
- Haffner, L. M., Dettmar, R.-J., Beckman, J. E., Wood, K., Slavin, J. D., Giammanco, C., Madsen, G. J., Zurita, A., & Reynolds, R. J. 2009, *Reviews of Modern Physics*, 81, 969
- Herwig, F. 2004, *ApJS*, 155, 651
- Hirschi, R., Meynet, G., & Maeder, A. 2005, *A&A*, 433, 1013
- Hsu, W.-H., Putman, M. E., Heitsch, F., Stanimirović, S., Peek, J. E. G., & Clark, S. E. 2011, *AJ*, 141, 57
- Hummels, C. B., Bryan, G. L., Smith, B. D., & Turk, M. J. 2013, *MNRAS*, 430, 1548
- Ilbert, O., McCracken, H. J., Le Fèvre, O., Capak, P., Dunlop, J., Karim, A., Renzini, M. A., Caputi, K., Boissier, S., Arnouts, S., Aussel, H., Comparat, J., Guo, Q., Hudelot, P., Kartaltepe, J., Kneib, J. P., Krogager, J. K., Le Floch, E., Lilly, S., Mellier, Y., Milvang-Jensen, B., Moutard, T., Onodera, M., Richard, J., Salvato, M., Sanders, D. B., Scoville, N., Silverman, J. D., Taniguchi, Y., Tasca, L., Thomas, R., Toft, S., Tresse, L., Vergani, D., Wolk, M., & Zirm, A. 2013, *A&A*, 556, A55
- Jenkins, E. B. 2009, *ApJ*, 700, 1299
- Karakas, A. I. 2010, *MNRAS*, 403, 1413
- Karakas, A. I., García-Hernández, D. A., & Lugaro, M. 2012, *ApJ*, 751, 8
- Kaufmann, T., Bullock, J. S., Maller, A. H., Fang, T., & Wadsley, J. 2009, *MNRAS*, 396, 191
- Kennicutt, Jr., R. C., Armus, L., Bendo, G., Calzetti, D., Dale, D. A., Draine, B. T., Engelbracht, C. W., Gordon, K. D., Helou, G., Hollenbach, D. J., Jarrett, T. H., Kewley, L. J., Leitherer, C., Li, A., Malhotra, S., Regan, M. W., Rieke, G. H., Rieke, M. J., Roussel, H., Smith, J.-D. T., Thornley, M. D., & Walter, F. 2003, *PASP*, 115, 928
- Kewley, L. J. & Dopita, M. A. 2002, *ApJS*, 142, 35
- Kewley, L. J. & Ellison, S. L. 2008, *ApJ*, 681, 1183
- Kroupa, P. 2001, *MNRAS*, 322, 231
- Lehner, N. & Howk, J. C. 2011, *Science*, 334, 955
- Lehner, N., Howk, J. C., Thom, C., Fox, A. J., Tumlinson, J., Tripp, T. M., & Meiring, J. D. 2012, *MNRAS*, 424, 2896
- Lehner, N., O'Meara, J. M., Fox, A. J., Howk, J. C., Prochaska, J. X., Burns, V., & Armstrong, A. A. 2014, arXiv:1401.1811
- Leitner, S. N. 2012, *ApJ*, 745, 149
- Leroy, A. K., Walter, F., Brinks, E., Bigiel, F., de Blok, W. J. G., Madore, B., & Thornley, M. D. 2008, *AJ*, 136, 2782
- Lockman, F. J., Murphy, E. M., Petty-Powell, S., & Urlick, V. J. 2002, *ApJS*, 140, 331
- Lodders, K., Palme, H., & Gail, H.-P. 2009, *Landolt Börnstein*, 44
- Madau, P., Ferguson, H. C., Dickinson, M. E., Giavalisco, M., Steidel, C. C., & Fruchter, A. 1996, *MNRAS*, 283, 1388
- Mannucci, F., Cresci, G., Maiolino, R., Marconi, A., & Gnerucci, A. 2010, *MNRAS*, 408, 2115
- Maoz, D. & Mannucci, F. 2012, *PASA*, 29, 447
- Marigo, P. 2001, *A&A*, 370, 194
- Matteucci, F. & Greggio, L. 1986, *A&A*, 154, 279
- McGaugh, S. S. 2005, *ApJ*, 632, 859
- , 2012, *AJ*, 143, 40
- Ménard, B. & Fukugita, M. 2012, *ApJ*, 754, 116
- Ménard, B., Nestor, D., Turnshek, D., Quider, A., Richards, G., Chelouche, D., & Rao, S. 2008, *MNRAS*, 385, 1053
- Ménard, B., Scranton, R., Fukugita, M., & Richards, G. 2010, *MNRAS*, 405, 1025
- Moster, B. P., Somerville, R. S., Maulbetsch, C., van den Bosch, F. C., Macciò, A. V., Naab, T., & Oser, L. 2010, *ApJ*, 710, 903
- Moustakas, J., Coil, A. L., Aird, J., Blanton, M. R., Cool, R. J., Eisenstein, D. J., Mendez, A. J., Wong, K. C., Zhu, G., & Arnouts, S. 2013, *ApJ*, 767, 50
- Muller, C. A., Oort, J. H., & Raimond, E. 1963, *Academie des Sciences Paris Comptes Rendus*, 257, 1661
- Murray, N., Quataert, E., & Thompson, T. A. 2005, *ApJ*, 618, 569
- Narayanan, A., Savage, B. D., Wakker, B. P., Danforth, C. W., Yao, Y., Keeney, B. A., Shull, J. M., Sembach, K. R., Froning, C. S., & Green, J. C. 2011, *ApJ*, 730, 15
- Nicholls, D. C., Dopita, M. A., & Sutherland, R. S. 2012, *ApJ*, 752, 148

- Noordermeer, E., van der Hulst, J. M., Sancisi, R., Swaters, R. A., & van Albada, T. S. 2005, *A&A*, 442, 137
- Oey, M. S., Meurer, G. R., Yelda, S., Furst, E. J., Caballero-Nieves, S. M., Hanish, D. J., Levesque, E. M., Thilker, D. A., Walth, G. L., Bland-Hawthorn, J., Dopita, M. A., Ferguson, H. C., Heckman, T. M., Doyle, M. T., Drinkwater, M. J., Freeman, K. C., Kennicutt, Jr., R. C., Kilborn, V. A., Knezek, P. M., Koribalski, B., Meyer, M., Putman, M. E., Ryan-Weber, E. V., Smith, R. C., Staveley-Smith, L., Webster, R. L., Werk, J., & Zwaan, M. A. 2007, *ApJ*, 661, 801
- Oppenheimer, B. D. & Davé, R. 2006, *MNRAS*, 373, 1265
- 2008, *MNRAS*, 387, 577
- Oppenheimer, B. D., Davé, R., Katz, N., Kollmeier, J. A., & Weinberg, D. H. 2012, *MNRAS*, 420, 829
- Origlia, L., Ranalli, P., Comastri, A., & Maiolino, R. 2004, *ApJ*, 606, 862
- Pagel, B. E. J. 2008, in *Astronomical Society of the Pacific Conference Series*, Vol. 390, *Pathways Through an Eclectic Universe*, ed. J. H. Knapen, T. J. Mahoney, & A. Vazdekis, 483
- Papastergis, E., Cattaneo, A., Huang, S., Giovanelli, R., & Haynes, M. P. 2012, *ApJ*, 759, 138
- Pasquali, A., Gallazzi, A., Fontanot, F., van den Bosch, F. C., De Lucia, G., Mo, H. J., & Yang, X. 2010, *MNRAS*, 407, 937
- Pasquali, A., Gallazzi, A., & van den Bosch, F. C. 2012, *MNRAS*, 425, 273
- Peebles, M. S. & Shankar, F. 2011, *MNRAS*, 417, 2962
- Peebles, M. S. & Somerville, R. S. 2013, *MNRAS*, 428, 1766
- Pettini, M. 1999, in *Chemical Evolution from Zero to High Redshift*, ed. J. R. Walsh & M. R. Rosa, 233
- Portinari, L., Chiosi, C., & Bressan, A. 1998, *A&A*, 334, 505
- Prochaska, J. X., Gawiser, E., Wolfe, A. M., Castro, S., & Djorgovski, S. G. 2003, *ApJ*, 595, L9
- Prochaska, J. X., Weiner, B., Chen, H.-W., Mulchaey, J., & Cooksey, K. 2011, *ApJ*, 740, 91
- Putman, M. E., Peek, J. E. G., & Joung, M. R. 2012, *ARA&A*, 50, 491
- Saintonge, A., Kauffmann, G., Kramer, C., Tacconi, L. J., Buchbender, C., Catinella, B., Fabello, S., Graciá-Carpio, J., Wang, J., Cortese, L., Fu, J., Genzel, R., Giovanelli, R., Guo, Q., Haynes, M. P., Heckman, T. M., Krumholz, M. R., Lemonias, J., Li, C., Moran, S., Rodríguez-Fernández, N., Schiminovich, D., Schuster, K., & Sievers, A. 2011, *MNRAS*, 415, 32
- Salpeter, E. E. 1955, *ApJ*, 121, 161
- Savage, B. D., Lehner, N., & Narayanan, A. 2011, *ApJ*, 743, 180
- Scannapieco, C., Tissera, P. B., White, S. D. M., & Springel, V. 2006, *MNRAS*, 371, 1125
- Sembach, K. R., Howk, J. C., Ryans, R. S. I., & Keenan, F. P. 2000, *ApJ*, 528, 310
- Shapley, A. E., Steidel, C. C., Pettini, M., & Adelberger, K. L. 2003, *ApJ*, 588, 65
- Shen, S., Madau, P., Aguirre, A., Guedes, J., Mayer, L., & Wadsley, J. 2012, *ApJ*, 760, 50
- Shen, S., Wadsley, J., & Stinson, G. 2010, *MNRAS*, 407, 1581
- Shull, J. M., Jones, J. R., Danforth, C. W., & Collins, J. A. 2009, *ApJ*, 699, 754
- Shull, J. M., Stevans, M., Danforth, C., Penton, S. V., Lockman, F. J., & Arav, N. 2011, *ApJ*, 739, 105
- Shull, J. M. 2014, arXiv:1401.5799
- Skibba, R. A., Engelbracht, C. W., Dale, D., Hinz, J., Zibetti, S., Crocker, A., Groves, B., Hunt, L., Johnson, B. D., Meidt, S., Murphy, E., Appleton, P., Armus, L., Bolatto, A., Brandl, B., Calzetti, D., Croxall, K., Galametz, M., Gordon, K. D., Kennicutt, R. C., Koda, J., Krause, O., Montiel, E., Rix, H.-W., Roussel, H., Sandstrom, K., Sauvage, M., Schinnerer, E., Smith, J. D., Walter, F., Wilson, C. D., & Wolfire, M. 2011, *ApJ*, 738, 89
- Sofia, U. J. & Meyer, D. M. 2001, *ApJ*, 554, L221
- Sonnenfeld, A., Treu, T., Gavazzi, R., Marshall, P. J., Auger, M. W., Suyu, S. H., Koopmans, L. V. E., & Bolton, A. S. 2012, *ApJ*, 752, 163
- Stinson, G. S., Brook, C., Prochaska, J. X., Hennawi, J., Shen, S., Wadsley, J., Pontzen, A., Couchman, H. M. P., Quinn, T., Macciò, A. V., & Gibson, B. K. 2012, *MNRAS*, 425, 1270
- Stocke, J. T., Keeney, B. A., Danforth, C. W., Shull, J. M., Froning, C. S., Green, J. C., Penton, S. V., & Savage, B. D. 2013, *ApJ*, 763, 148
- Swaters, R. A. & Balcells, M. 2002, *A&A*, 390, 863
- Thielemann, F.-K., Nomoto, K., & Yokoi, K. 1986, *A&A*, 158, 17
- Thom, C., Peek, J. E. G., Putman, M. E., Heiles, C., Peek, K. M. G., & Wilhelm, R. 2008, *ApJ*, 684, 364
- Thom, C., Tumlinson, J., Werk, J. K., Prochaska, J. X., Oppenheimer, B. D., Peebles, M. S., Tripp, T. M., Katz, N. S., O'Meara, J. M., Brady Ford, A., Davé, R., Sembach, K. R., & Weinberg, D. H. 2012, *ApJ*, 758, L41
- Thomas, D., Maraston, C., Bender, R., & Mendes de Oliveira, C. 2005, *ApJ*, 621, 673
- Tinsley, B. M. 1979, *ApJ*, 229, 1046
- Tsujimoto, T., Nomoto, K., Yoshii, Y., Hashimoto, M., Yanagida, S., & Thielemann, F.-K. 1995, *MNRAS*, 277, 945
- Tumlinson, J., Thom, C., Werk, J. K., Prochaska, J. X., Tripp, T. M., Katz, N., Davé, R., Oppenheimer, B. D., Meiring, J. D., Ford, A. B., O'Meara, J. M., Peebles, M. S., Sembach, K. R., & Weinberg, D. H. 2013, *ApJ*, 777, 59
- Tumlinson, J., Thom, C., Werk, J. K., Prochaska, J. X., Tripp, T. M., Weinberg, D. H., Peebles, M. S., O'Meara, J. M., Oppenheimer, B. D., Meiring, J. D., Katz, N. S., Davé, R., Ford, A. B., & Sembach, K. R. 2011, *Science*, 334, 948
- Wakker, B. P., York, D. G., Howk, J. C., Barentine, J. C., Wilhelm, R., Peletier, R. F., van Woerden, H., Beers, T. C., Ivezić, Ž., Richter, P., & Schwarz, U. J. 2007, *ApJ*, 670, L113
- Wakker, B. P., York, D. G., Wilhelm, R., Barentine, J. C., Richter, P., Beers, T. C., Ivezić, Ž., & Howk, J. C. 2008, *ApJ*, 672, 298
- Weiner, B. J., Coil, A. L., Prochaska, J. X., Newman, J. A., Cooper, M. C., Bundy, K., Conselice, C. J., Dutton, A. A., Faber, S. M., Koo, D. C., Lotz, J. M., Rieke, G. H., & Rubin, K. H. R. 2009, *ApJ*, 692, 187
- Weingartner, J. C. & Draine, B. T. 2001, *ApJ*, 548, 296
- Weisz, D. R., Dalcanton, J. J., Williams, B. F., Gilbert, K. M., Skillman, E. D., Seth, A. C., Dolphin, A. E., McQuinn, K. B. W., Gogarten, S. M., Holtzman, J., Rosema, K., Cole, A., Karachentsev, I. D., & Zaritsky, D. 2011, *ApJ*, 739, 5
- Werk, J. K., Prochaska, J. X., Thom, C., Tumlinson, J., Tripp, T. M., O'Meara, J. M., & Meiring, J. D. 2012, *ApJS*, 198, 3
- Werk, J. K., Prochaska, J. X., Thom, C., Tumlinson, J., Tripp, T. M., O'Meara, J. M., & Peebles, M. S. 2013, *ApJS*, 204, 17
- Werk, J. K., Putman, M. E., Meurer, G. R., & Santiago-Figueroa, N. 2011, *ApJ*, 735, 71
- West, A. A., Garcia-Appadoo, D. A., Dalcanton, J. J., Disney, M. J., Rockosi, C. M., & Ivezić, Ž. 2009, *AJ*, 138, 796
- West, A. A., Garcia-Appadoo, D. A., Dalcanton, J. J., Disney, M. J., Rockosi, C. M., Ivezić, Ž., Bentz, M. C., & Brinkmann, J. 2010, *AJ*, 139, 315
- Whittet, D. C. B. 2010, *ApJ*, 710, 1009
- Woo, J., Courteau, S., & Dekel, A. 2008, *MNRAS*, 390, 1453
- Woodsley, S. E. & Weaver, T. A. 1995, *ApJS*, 101, 181
- Worthey, G., Faber, S. M., & Gonzalez, J. J. 1992, *ApJ*, 398, 69
- Yan, R. & Blanton, M. R. 2012, *ApJ*, 747, 61
- Yao, Y., Wang, Q. D., Penton, S. V., Tripp, T. M., Shull, J. M., & Stocke, J. T. 2010, *ApJ*, 716, 1514
- Zahid, H. J., Bresolin, F., Kewley, L. J., Coil, A. L., & Davé, R. 2012a, *ApJ*, 750, 120
- Zahid, H. J., Dima, G. I., Kewley, L. J., Erb, D. K., & Davé, R. 2012b, *ApJ*, 757, 54
- Zhang, W., Li, C., Kauffmann, G., Zou, H., Catinella, B., Shen, S., Guo, Q., & Chang, R. 2009, *MNRAS*, 397, 1243
- Zu, Y., Weinberg, D. H., Davé, R., Fardal, M., Katz, N., Kereš, D., & Oppenheimer, B. D. 2011, *MNRAS*, 412, 1059
- Zubko, V., Dwek, E., & Arendt, R. G. 2004, *ApJS*, 152, 211

## APPENDIX

## AN ACCOUNTING OF OXYGEN

As the production sites of the different elements (Figure 2) differ, the eventual fate of different elements should also differ (Tinsley 1979; Matteucci & Greggio 1986). We attempt here to address how the census of the most abundant heavy element, oxygen, differs from that of “all metals”. In most cases, we have either derived metal masses from oxygen (e.g., ISM gas or the O VI-traced CGM), and / or we lack the sensitivity to non-Solar abundance patterns (e.g., the low-ionization or X-ray traced CGM). With both stars (§ A.1) and dust (§ A.2), however, we can begin to address the elemental distribution of metals.

*Oxygen in Stars*

Where the stellar abundances of  $\alpha$ -elements (of which oxygen is one, along with, e.g., Mg, Si, Ne, etc.) have been measured relative to stellar Fe abundances, massive galaxies have been found to be more  $\alpha$ -enhanced than less massive galaxies (e.g., Worthey et al. 1992; Thomas et al. 2005). As done by Peebles & Somerville (2013) we therefore renormalize the Gallazzi et al. (2005) data according to the relation fit to data from Arrigoni et al. (2010),

$$[\alpha/\text{Fe}] = 0.085 + 0.062(\log M_\star/M_\odot - 10), \quad (\text{A1})$$

with a  $\sigma$ -to- $M_\star$  conversion as measured by Thomas et al. 2005, where  $[\alpha/\text{Fe}]$  is the logarithm of the ratio of the abundance of  $\alpha$ -elements to the abundance of iron, where  $[\alpha/\text{Fe}] = 0$  is the solar ratio. We note that the normalization of this relation has decreased as the reference models have improved (Arrigoni et al. 2010; Conroy et al. 2013).

We apply this correction by assuming that the metals-to-iron and  $\alpha$ -to-oxygen ratios follow Solar abundance patterns.

We adopt a solar oxygen abundance of  $[12 + \log(\text{O}/\text{H})]_\odot = 8.76$  (Caffau et al. 2011). The uncertainty plotted in right-hand panel of Figure 1 includes the range of older estimates of 8.69 (Asplund et al. 2009) to 8.89 (Delahaye & Pinsonneault 2006). We further include the range in uncertainty for letting  $[\alpha/\text{Fe}] = 0$  for all galaxies; for most of this mass range, this is similar to adopting the higher oxygen abundance with a varying  $\alpha/\text{Fe}$  ratio. Because this correction is larger for more massive galaxies, the inferred uncertainty in the oxygen mass in stars is also larger.

*Oxygen in Dust*

We assume that 27% of dust is oxygen, by mass, with a possible error range of 22–35%. Using the Weingartner & Draine (2001), Zubko et al. (2004), and Draine & Fraisse (2009) dust models to constrain the oxygen fraction of dust (see also Draine 2011), we find

$$\frac{M_{\text{oxy,dust}}}{M_{\text{dust}}} = \frac{\mu_{\text{oxy}} N_{\text{dust}}^{\text{oxy}}}{\sum_X \mu_X N_{\text{dust}}^X}, \quad (\text{A2})$$

where  $\mu$  is the average atomic mass,  $X$  is one of the elements C, N, O, Mg, Si, and Fe, and  $N$  denotes the number abundance. In these three models,  $M_{\text{oxy,dust}}/M_{\text{dust}}$  is 25.1, 32.1, and 25.7%, respectively. We note that observational constraints on the oxygen mass fraction of dust from oxygen dust depletions are difficult to reconcile with chemical models (Sofia & Meyer 2001; Draine 2003; Jenkins 2009; Whittet 2010). Moreover, depletion studies generally imply that the oxygen-to-metals ratio in dust is as high as in the Sun.

As there are many other uncertainties we do not explicitly take into account, we show in Figure 1 a range of 22–35% with a best-guess of 27%, after adopting the mean dust relation given in Equation (14).

Finally, we note that this dust oxygen fraction of 27% is less than the Solar oxygen-to-metals ratio of 44%.

*Oxygen lost from galaxies*

We consider the oxygen lost from galaxies,

$$\Omega_{\text{oxy,lost}} = \frac{1}{\rho_c} \int_{M_{\star,\text{min}}}^{M_{\star,\text{max}}} M_{\text{oxy,lost}}(M_\star) \frac{dn(M_\star)}{d \log M_\star} d \log M_\star, \quad (\text{A3})$$

where

$$M_{\text{oxy,retain}}(M_\star) = M_{\text{oxy},\star} + M_{\text{oxy,ism}} + M_{\text{oxy,dust}}. \quad (\text{A4})$$

The right panel of Figure 11 shows  $f_{\text{oxy,retain}} \equiv M_{\text{oxy,retain}}/M_{\text{oxy,made}}$  v.  $\log M_\star$ . The increase in  $f_{\text{oxy,retain}}$  relative to the metals available fraction is entirely driven by the increase in the stellar  $[\alpha/\text{Fe}]$  with stellar mass; unlike for metals, the uncertainties in this fraction are not dominated by the yield uncertainties, but rather roughly equal contributions of stellar and ISM, with the uncertainty in the oxygen dust fraction entering at larger stellar masses. This large difference is particularly surprising since if the abundance ratios of star-formation driven outflows differ from solar, they are probably  $\alpha$ -enhanced, implying that  $[\alpha/\text{Fe}]$  *outside* of galaxies should also be greater than in the sun. One

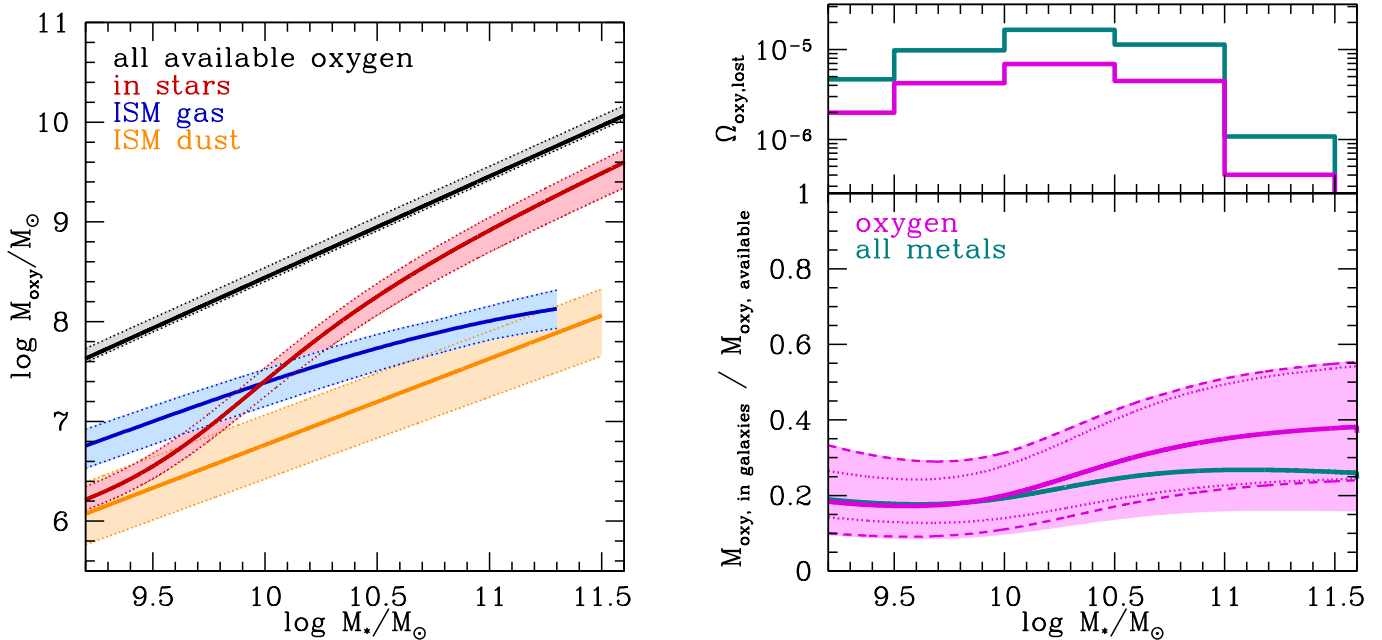


**Figure 11.** *Left:* Same as Figure 1, but for just oxygen. *Right:* Same as Figure 5, but for oxygen. The increase in  $f_{\text{oxy, retain}}$  at high  $M_{*}$  is nearly entirely due to the increase in  $[\alpha/\text{Fe}]$  in stars.

possible solution to this conundrum is that the ISM might not have solar abundance ratios, or have  $[\alpha/\text{Fe}]$  ratios that also depend on stellar mass; here, we measure the ISM *oxygen* mass, but infer its metal mass by assuming a solar oxygen-to-metals ratio. If the ISM is  $\alpha$ -depleted for the  $M_{*} \gtrsim 10^{10.5} M_{\odot}$  galaxies, then the shape of  $f_{Z, \text{retain}}(M_{*})$  might have a shape similar to  $f_{\text{oxy, retain}}(M_{*})$  rather than being so surprisingly flat.

#### *Circumgalactic Oxygen and the “Missing Oxygen Problem”*

If outflows are preferentially  $\alpha$ -enhanced (e.g., because they are driven by Type II supernovae), then the CGM might have a higher Oxygen-to-metals ratio than found in the Sun. The  $[\alpha/\text{Fe}]$  ratio for circumgalactic gas, however, is not yet able to be measured, and so for the time being we must assume Solar Oxygen-to-metals ratios. An “ $\alpha$ -enhanced” CGM would decrease our O VI-derived metal masses, but it is superficially unclear how a higher SN II contribution would affect the metal masses we derive for the low-ionization CGM. As shown in Figure 12, we take the O VI-traced oxygen mass given in Equation (24), and take a Solar oxygen-to-metals ratio of 0.44 for the low-ionization and X-ray traced CGM components (though see Origlia et al. 2004). For circumgalactic dust, we assume CGM dust has a similar chemistry to that of ISM dust, with a dust oxygen mass fraction of 27% (§ A.2). (Given the uncertainties in how dust can survive in first a wind fluid and subsequently in the CGM, it is unlikely that circumgalactic dust has a similar chemistry to interstellar dust, but there is currently no conclusive evidence one way or the other.)

With regards to the “missing oxygen problem” (Figure 13), the picture is a little more complicated than for all metals. The uncertainties in the oxygen masses at the high- $M_{*}$  end are dominated by the uncertainty in the stellar  $[\alpha/\text{Fe}]$  in star-forming galaxies. The observed dependence on the stellar  $\alpha$ -enhancement in passive galaxies (Thomas et al. 2005; Arrighi et al. 2010) is generally attributed to an age dependence. Within the mass range of the star-forming population we consider here, however, there is still expected to be an age-mass relation that should also manifest as a correlation between  $[\alpha/\text{Fe}]$  and  $M_{*}$ , though it would be surprising if this relation is the same as for passive galaxies. Likewise, if supernovae are significant drivers of redistributing metals into the CGM, then it is quite possible that the CGM could be  $\alpha$ -enriched while the ISM is left  $\alpha$ -depleted; the current observations are not sensitive to these differences.

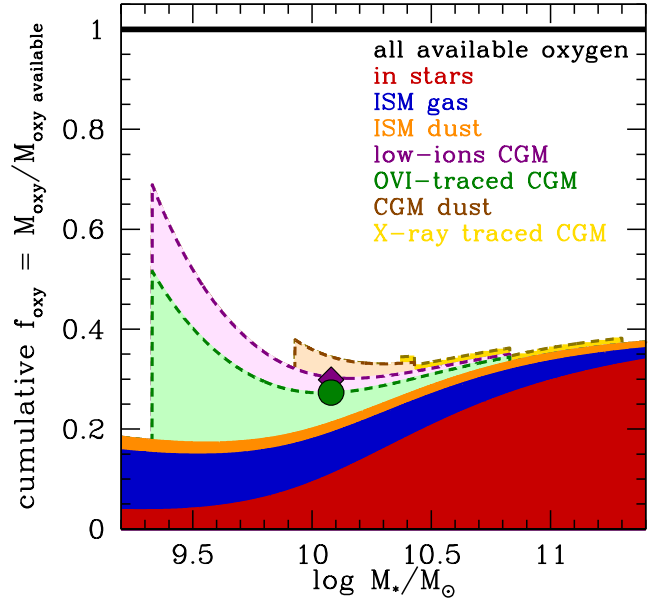
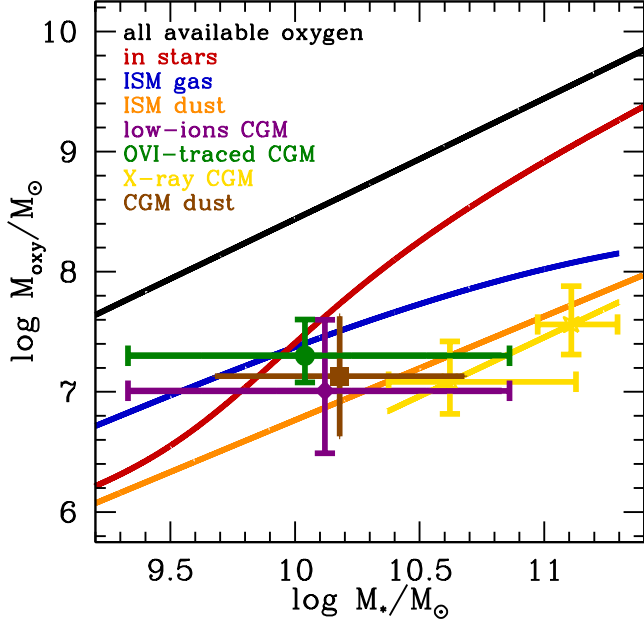


Figure 12. Same as Figure 9 but for oxygen.

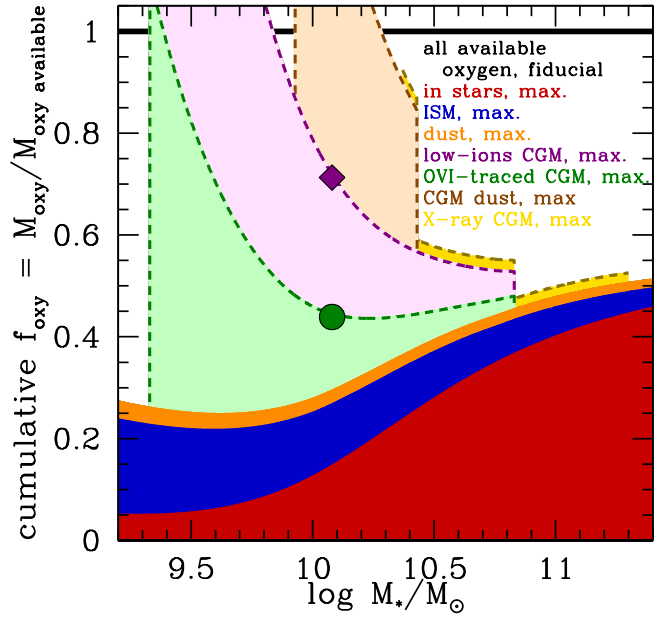
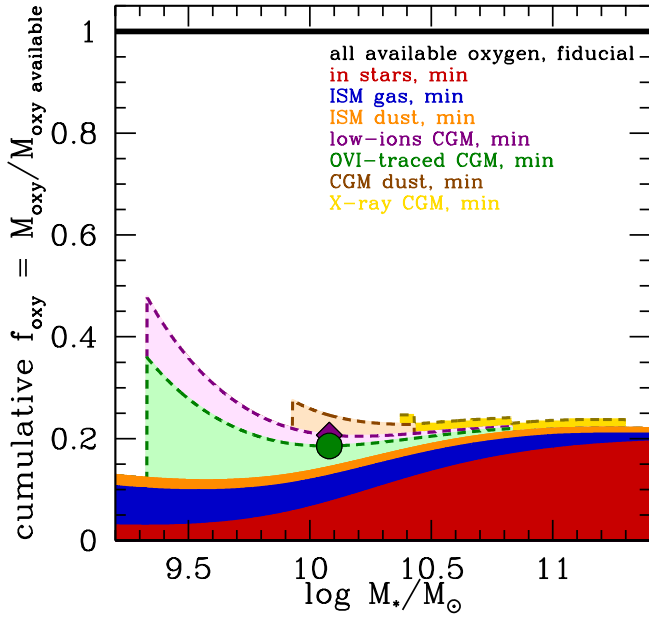


Figure 13. Same as Figure 10 but for oxygen.